Università degli Studi di Milano-Bicocca
Facoltà di Scienze Matematiche, Fisiche e Naturali
Corso di Laurea Specialistica in Fisica

Exchange and Correlation effects in the electronic properties of transition metal oxides: the example of NiO

Relatore interno: **Prof. Giorgio Benedek**
Relatrice esterna: **Dr.ssa Lucia Reining**
Correlatore esterno: **Dr. Matteo Gatti**

Tesi di Laurea di
Matteo Guzzo
Matricola 055692

III Sessione
Anno Accademico 2007-2008

A Clara, Gigi, Fabio, Alice

La misura di amare
è di amare senza misura

Contents

Chapter 1

Introduction

THE PURPOSE OF THIS WORK is to investigate the role of exchange and correlation effects on the electronic structure of nickel oxide, namely on the nature of the insulating energy-gap, by means of ab-initio methods. *Ab-initio* methods, also know as *first-principles* methods, are parameter-free approaches. They start from the all-electron many-body Hamiltonian and try to solve it in a consistent way, without introducing any external arbitrary or fitted parameter. They of course must introduce approximations that permit to solve the problem in practice. In most cases ground-state properties of electronic systems are well described by Density-Functional Theory [1]. The Kohn-Sham scheme [2] (used to solve DFT in practice) has been unproperly used to describe also excited states properties, like band structures and energy-gaps. This uncorrect approach was often the only affordable one and it has given surprisingly good results for many compounds. As a matter of fact, the independent-electron picture has been successful in describing the properties of a lot of materials and has marked the early developement of solid-state physics. Still, it is a crude approximation. In fact, there is a particular class of materials that has underpinned the limits of this approximation. These materials are often called *strongly-correlated* and display a wide range of important properties from both a fundamental and technological point of view, ranging from colossal magnetoresistance to high temperature superconductivity. Among them there are transition-metal oxides. Transition-metal monoxides like NiO are of particular interest in this framework as prototype systems. Lately, great attention has been drawn to *correlation effects* in strongly-correlated materials. In solid state physics books, *correlation* is defined as *"everything that goes beyond the Hartree-Fock approximation"*. At first sight, this definition does not give a clue about the physical meaning of correlation. Electronic correlation is the fact that in a many-electron system, like a molecule or a bulk solid, the electrons cannot be depicted as "almost free", i.e. independent and surrounded by an effective poten-

tial that accounts for all interactions with other electrons. These interactions — the *correlation effects* — namely affect excited-states properties.

Direct and inverse photoemission experiments are the most direct experimental way to measure the band structure of solids. They investigate $N-1$ and $N+1$ particles excited states and hence need a theory able to describe changes in the number of particles of the system.[1] This is the case of Many-Body Perturbation Theory (MBPT), that treats the electronic problem in terms of n-particle propagators or *Green's functions* [3]. Namely, the key quantity in photoemission is the one-particle Green's function while for absorption spectra, which involve neutral excitations, the key quantity one has to calculate is the two-particle Green's function. A tractable approach derived from MBPT is the *GW* approximation [4, 5]. This approach allows one to calculate electron addition and removal energies, i.e the photoemission spectra.

Correlation effects in photoemission spectra are related to the *screening*, which finds its analytic expression in the dielectric function ε^{-1}. The dielectric function describes how the system reacts to an external field. The meaning of ε^{-1} can be linked to the Hartree-Fock approximation via the *GW* approximation. In H-F, the Koopmans' theorem [6] is supposed to be valid. The Koopmans' theorem states that H-F energies correspond to the particle removal (addition) energies in a direct (inverse) photoemission experiment, provided that there is no relaxation of the other electrons. In H-F the key interaction is the bare Coulomb interaction v, that is a static (i.e. time-independent) interaction. On the other hand, in the *GW* approximation the key interaction is $W = \varepsilon^{-1}v$, that is the *dynamical screened Coulomb interaction*. It turns out that the Hartree-Fock approximation can be seen as a particular case of *GW* in the limit of $\varepsilon^{-1} = 1$. This explains the link between screening and correlation and clears out the first definition of correlation. In *GW*, neglecting correlation means neglecting the screening, i.e. being in the Hartree-Fock limit.

Taking Hartree-Fock as a reference, two main correlation effects can be found in photoemission spectra calculated in the *GW* approximation: the energy peak is found at different energies and it is broadened with respect to H-F peaks. This means that the excited state's lifetime is finite, as it is proportional to the inverse of the FWHM of the peak. There are also additional structures, called satellites, that are related to collective excitations, e.g. *plasmons*.

On the other side of correlation, there is *exchange*. Exchange is the fact that different electrons, because of their quantum nature, cannot be distinguished from each other when they are close together and their wave functions *overlap*. This has a direct consequence on the symmetry of the many-body wavefunction. Ex-

[1] The charged excitation energy for an N-particle system is defined as $E_{\text{exc}} = E_N - E_{N\pm1}$ if a particle is being added or removed respectively.

change is exactly described in Hartree-Fock approximation where any direct electron–electron interaction is neglected. In this sense, the Hartree-Fock method can be a reference to distinguish exchange from correlation effects, which could sometimes be mistaken one another.

Nickel oxide is an insulator with a photoemission gap of 4.3 eV. At room temperature, it is a type-II antiferromagnet. At 523 K, it undergoes a magnetic transition from antiferromagnetic to paramagnetic. The photoemission gap and spectrum are not affected by the magnetic transition [7, 8]. As a prototype of strongly-correlated materials, the electronic structure of nickel oxide has been extensively studied, within several experimental and theoretical methods and models [7–28]. However, the origin of its gap is still under debate. Some people [7, 10, 16] claim it to be a Mott insulator, while others state that it can be described in a band-structure framework, even though the description of the paramagnetic phase is problematic in the latter case [18–21]. The debate between the two communities is still open.

In this thesis both paramagnetic and antiferromagnetic phases are covered. In Chapter 3 I investigate the role of exchange effects on the paramagnetic phase of NiO by means of the Hartree-Fock approximation. In Chapter 4 I take care of the antiferromagnetic phase by means of MBPT techniques. Following a new approach on nickel oxide, focused at describing properly the photoemission gap and spectrum, I discuss the nature of the insulating gap in NiO and the role of exchange and correlation effects.

Chapter 2

Theoretical framework

In this chapter I will present all the tools that I have been using to approach the problem of electronic structure in solids during my thesis work. Starting from the Density-Functional Theory [1] (DFT), which has the electronic density as the key variable of the system, I will proceed in describing the Green's functions method, or Many-Body Perturbation Theory (MBPT), which relies on the Green's function as the key element to solve the electronic problem. I will also carry out a discussion on the need of a proper method to calculate photoemission spectra, such as the *GW* method.

Throughout the thesis, I will make use of a number of conventional notations and units. Hartree atomic units will be used in formulas, i.e. $e^2 = \hbar = m = 1$. Energies are also expressed in Hartree units (1 Hartree = 27.2114 eV) and lengths are expressed in units of the Bohr radius (1 Bohr=0.52918 Å). In the section about Green's functions theory shorthands for $\psi(\mathrm{r}_1, \sigma_1, t_1)$ and $d\mathrm{r}_1 d\sigma_1 dt_1$ inside integrals will be used, namely $\psi(1)$ and $d1$.

2.1 The many-body electron problem

In quantum mechanics the full Hamiltonian of a system of ions and electrons is the following:

$$\hat{H} = -\sum_i^N \frac{\nabla_i^2}{2} - \sum_I^M \frac{\nabla_I^2}{2M_I} + \sum_{i<j}^N \frac{1}{|\mathbf{r}_i - \mathbf{r}_j|} + \\ - \sum_i^N \sum_I^M \frac{Z_I}{|\mathbf{r}_i - \mathbf{R}_I|} + \sum_{I<J}^M \frac{Z_I Z_J}{|\mathbf{R}_I - \mathbf{R}_J|}$$

where I and $\mathbf{R}_I$ are the ion index and position and M the number of ions; i and $\mathbf{r}_i$ are the electron index and position and N is the number of electrons. M_I is

I-th ion's mass and Z_I is I-th ion's atomic number. The system is ruled by the Schrödinger equation:

$$\hat{H}\Psi(\mathbf{r},\mathbf{R}) = E\Psi(\mathbf{r},\mathbf{R}).$$

The complexity of the system described by this Hamiltonian is far too big to permit an easy resolution. A first approximation is the so-called *adiabatic* or Born-Oppenheimer approximation, which consists in separating the motion of the electrons from the ions. This approximation is based on the assumption that the electrons are much faster than the nuclei (their speed ratio is proportional to the inverse of their mass ratio, i.e. $\sim 10^3$). So the electronic problem alone can be analyzed for each given ionic configuration.

We shall then take the electronic Hamiltonian for the stationary problem, $\mathcal{H}$:

$$\mathcal{H} = \sum_i^N \left(-\frac{\nabla_i^2}{2} + V_{\text{ext}}(\mathbf{r}_i) \right) + \sum_{i<j}^N v_{ij} \tag{2.1}$$

where $v_{ij} = \frac{1}{|\mathbf{r}_i - \mathbf{r}_j|}$ is the Coulomb term of the potential and $V_{\text{ext}}(\mathbf{r}_i)$ is the sum of the ionic potential and of the external potential. Resolving exactly the corresponding Hamilton equation is an impossible task, at least in the time of a human life. Nevertheless, we have now a starting point which can be treated by means of different (alas, necessary) approximations.

2.2 Density-Functional Theory

Density-Functional Theory (Hereafter DFT) is a ground-state theory in which the emphasis is on the charge density as the relevant physical quantity [1]. DFT has proved to be highly successful in describing structural and electronic properties in a vast class of materials, ranging from atoms and molecules to simple crystals to complex extended systems (including glasses and liquids). Furthermore DFT is computationally relatively simple with respect to other wavefunction-based methods like Hartree-Fock or MP2 and MP3 (very popular among quantum chemists, since their applicability is limited to isolated systems). DFT is computationally cheap because its standard application implies the diagonalization of an independent-particle-type Hamiltonian where the potential is local and density-dependent. For these reasons DFT has become a common tool in first-principles calculations aimed at describing — or even predicting — properties of molecular and condensed matter systems. DFT is based on the Hohenberg-Kohn theorem. This theorem states that there is a one-to-one relation between a ground-state observable of an electronic system (like the energy) and the ground-state electronic density. If one knew the exact functional of the density, he would be able to calculate every observable for a given density. Thus there would be no need to calculate

the many-body wavefunction, which is much more complicated to compute than the density and carries much more information, of which only a small part is actually needed to calculate the ground-state observables.

Here we summarize the Hohenberg-Kohn theorem [1]. There is a one-to-one relation between the electronic density and groundstate wavefunctions. The energy density functional is so defined:

$$E[n] = \langle \Psi[n] | \mathcal{H} | \Psi[n] \rangle, \tag{2.2}$$

where $\Psi[n]$ is the groundstate Ψ_0 in some external potential. $\mathcal{H}$ is the Hamiltonian of the system (2.1). The energy can be expressed as a functional of the density:

$$E[n] = \int d\mathbf{r} n(\mathbf{r}) v_{ext}(\mathbf{r}) + F[n] \tag{2.3}$$

and it is minimal with respect to n with minimum n_0 (the ground-state electron density):

$$E_0 = E(n_0) < E(n), \quad n(\mathbf{r}) \neq n_0(\mathbf{r}). \tag{2.4}$$

$F[n]$ is an universal functional of the density and it does not depend on the external potential.

A practical application of the DFT is possible thanks to the Kohn-Sham scheme [2]. Kohn and Sham stated that it is possible to define a non-interacting electronic system with an effective potential that has exactly the same density of the interacting one. This system is usually referred to as the Kohn-Sham system. The density is thus defined as:

$$n(\mathbf{r}) = \sum_{i=1}^{N} |\phi_i(\mathbf{r})|^2 \tag{2.5}$$

where $\phi_i(\mathbf{r})$ are the single-particle wavefunctions and are called the Kohn-Sham orbitals. The Kohn-Sham equations are the following:

$$\left(-\frac{\nabla^2}{2} + V_{\text{eff}}(\mathbf{r}) - \epsilon_i \right) \phi_i(\mathbf{r}) = 0 \tag{2.6}$$

This effective potential is composed by three different parts:

$$V_{\text{eff}}(\mathbf{r}) = V_{\text{ext}}(\mathbf{r}) + \int \frac{n(\mathbf{r}')}{|\mathbf{r} - \mathbf{r}'|} d\mathbf{r}' + V_{\text{xc}}(\mathbf{r}) \tag{2.7}$$

The exchange-correlation potential $V_{\text{xc}}(\mathbf{r})$ contains all the many-body electron interactions and it is defined as $V_{\text{xc}}(\mathbf{r}) = \frac{\delta E_{\text{xc}}}{\delta n(\mathbf{r})}$, where E_{xc} is the exchange-correlation

energy functional. This functional is linked to the Hohenberg-Kohn energy functional via the following formula

$$E[n] = T'[n] + \int d\mathbf{r} V_{\text{ext}}(\mathbf{r}) n(\mathbf{r}) + \frac{1}{2} \int \int \frac{n(\mathbf{r}) n(\mathbf{r}')}{|\mathbf{r} - \mathbf{r}'|} d\mathbf{r} d\mathbf{r}' + E_{\text{xc}}[n], \tag{2.8}$$

where $T'[n]$ is the total kinetic energy of the Kohn-Sham system (i.e. sum of the single-particle kinetic energies). The second and third term are the external field interaction energy and the electrostatic classical energy (*Hartree*) respectively. The *Local Density Approximation* (LDA) consists in neglecting the non-local dependence of the functional on the density $n(\mathbf{r})$, so re-defining the functional:

$$E_{\text{xc}}^{LDA} \equiv \int \epsilon_{\text{xc}}(n(\mathbf{r})) n(\mathbf{r}) d\mathbf{r}, \tag{2.9}$$

where ϵ_{xc} is the exchange-correlation energy per electron of a homogeneous electron gas with density n. The exact dependence of $E_{\text{xc}}[n]$ on n is a functional dependence. This means that in general the energy per particle in a point does not only depend on the value of the density in that point. Instead, it depends on the value of the density in all points (i.e. it is *non-local*). The LDA eliminates this problem with a very simple assumption that makes also the calculation cheaper. In fact, to calculate the energy one needs to know the density only in a given point and not all over space. The Kohn-Sham equations are solved self-conistently, minimizing the total energy of the system, and the form of the Kohn-Sham potential, which is local in space and depends only on the density, permits to reach the minimum in a much quicker way than e.g. the Hartree-Fock equations. In the latter case the calculation of the exchange operator, which is non-local, is the major computational drawback, while the effective potential in the Kohn-Sham is local.

Density-Functional theory, in its applicable form of the the Kohn-Sham equations, is the weapon of choice of solid-state physicists to calculate ground-state properties of most solids. Great success has come form its affordability and relatively good accuracy. However, the final aim of my work is to calculate a photoemission spectrum, i.e. excited-states properties. While DFT can accomplish most tasks regarding the ground-state properties, the calculation of photoemission spectra needs additional tools. Many-Body Perturbation Theory (MBPT) has a natural attitude in describing excited-state properties, since it has its own relevant physical quantity in the Green's function. The link between photoemission and one-particle Green's function $G(\mathrm{r}_1, t_1; \mathrm{r}_2, t_2)$ will be briefly traced in the next section.

2.3 Green's functions theory

What is a Green's function?

Green's functions are used in many different fields of physics and there defined in slightly different ways. The Green's function is here defined as the propagator of a particle (electron or hole) from space-time point 2 to space-time point 1[1]. This is actually the (time-ordered) one-particle Green's function, defined as follows:

$$iG(1,2) = \langle N|\mathcal{T}\left[\hat{\psi}(1)\hat{\psi}^{\dagger}(2)\right]|N\rangle = \begin{cases} \langle N|\hat{\psi}(1)\hat{\psi}^{\dagger}(2)|N\rangle & t_1 > t_2 \\ -\langle N|\hat{\psi}(2)^{\dagger}\hat{\psi}(1)|N\rangle & t_1 < t_2 \end{cases} \tag{2.10}$$

where $\hat{\psi}^{\dagger}(1)$ and $\hat{\psi}(1)$ are the 2nd-quantization field operators which operate in Fock's space in the Heisenberg representation. $\hat{\psi}^{\dagger}(1)$ is the creation operator. $\hat{\psi}(1)$ is the annihilation operator. Actually $\hat{\psi}(1)$ is an abbreviation for $\hat{\psi}(\mathbf{r}_1, \sigma_1, t_1)$. This notation will be used troughout the whole thesis. $\mathcal{T}$ is Wick's time-ordering operator, which orders the two field operators in the correct order, according to t_1 and t_2, following the definition in equation (2.10). $|N\rangle$ stands for $\Psi(\mathbf{r}_1, \sigma_1, \ldots, \mathbf{r}_N, \sigma_N, t)$, the ground-state N-particle many-body wavefunction. The one-particle Green's function brings all the information about one-particle properties of the system, namely:

- the expectation value of any single-particle ground-state operator (like the density);
- the ground-state energy of the system;
- the single-particle excitation spectrum (i.e. the photoemission spectrum).

We will see now how to find the expectation value of a generic observable once the Green's function is provided. Let us take a generic observable $J(1,2)$ (within the first quantization picture). In second quantization it can be rewritten as

$$\mathcal{J} = \int d12\delta(t_2 - t_1)\hat{\psi}^{\dagger}(1)J(1,2)\hat{\psi}(2). \tag{2.11}$$

The second-quantization ground-state expectation value is then given by

$$\begin{aligned} \langle N|\mathcal{J}|N\rangle &= \int d12\delta(t_2 - t_1)J(1,2)\langle N|\hat{\psi}^{\dagger}(1)\hat{\psi}(2)|N\rangle \\ &= -\int d12\delta(t_2 - t_1^{+})J(1,2)\langle N|\mathcal{T}\left[\hat{\psi}(2)\hat{\psi}^{\dagger}(1)\right]|N\rangle \end{aligned} \tag{2.12}$$

[1] To have a complete overview on Green's functions theory, see [3–5].

where t_1^+ stands for $t_1 + \delta$, with δ an infinitesimal positive real number. This has been done in order to introduce the time-ordering operator and recognize the definition of the Green's function given in (2.10). $\mathcal{J}$ can be then rewritten as:

$$\mathcal{J} = i \int d12\delta(t_2 - t_1^+) J(1,2) G(2,1). \tag{2.13}$$

This general example shows how the knowledge of the Green's function can give any single-particle operator's expectation value. As a further example, we can write the ground-state density:

$$n(1) = -iG(1, 1^+) \tag{2.14}$$

This last equation shows that the ground-state density is actually the one-particle Green's function's diagonal in space and time.

2.3.1 Lehmann's representation and the spectral function

We just gave a definition of the one-particle Green's function, but how can we calculate it? Of course not straightforwardly; we don't know the form of the many-body wavefunctions and of the field operators. We will now try to find another way to write the Green's functions that could help to calculate it and to get some physical insight of the problem.

We shall first introduce $N + 1$ and $N - 1$ excited states. Using their closure relations in the Fock space $\{|N, i\rangle\}$ and passing in Fourier's space, we can derive the so-called Lehmann's representation of one-particle Green's function [29]:

$$G(\mathbf{r}_1, \mathbf{r}_2, \omega) = \sum_i \frac{f_i(\mathbf{r}_1) f_i^*(\mathbf{r}_2)}{\omega - \epsilon_i + i\eta \,\text{signum}(\epsilon_i - \mu)} \tag{2.15}$$

where the term $i\eta \,\text{signum}(\epsilon_i - \mu)$ (with $\eta \to 0$ real and positive) is introduced to permit the Fourier trasform. Lehmann's amplitudes $f_i(\mathbf{r})$ are defined in the Fock space as:

$$f_i(\mathbf{r}) = \begin{cases} \langle N|\psi(\mathbf{r})|N+1, i\rangle & \epsilon_i > \mu \\ \\ \langle N-1, i|\psi(\mathbf{r})|N\rangle & \epsilon_i < \mu \end{cases} \tag{2.16}$$

and the one-particle excitation energies are:

$$\epsilon_i = E_{N+1,i} - E_N. \tag{2.17}$$

The form (2.15) of the Green's function points out its connection with the excitation energies. In fact, $G(\mathbf{r}_1, \mathbf{r}_2, \omega)$ is the sum over the i states of an $N + 1$ multi-particle state ($N - 1$ in case of holes) of its poles (which are the excitation

energies) weighted by Lehmann's amplitudes. The ϵ_i are electron addition and removal energies. Hence, the photoemission energies that are measured in direct and inverse photoemission spectroscopy are the poles of the one-particle Green's function. This shows how the Green's function is the proper tool to calculate the photoemission spectrum of a system.

The Green's function is a complex function. One may want to focus on the excitation energies. Knowing that $\lim_{\eta\to 0^+} \frac{1}{x+i\eta} = \mathcal{P}\frac{1}{x} - i\pi\delta(x)$ and applying it to (2.15) one could keep only its imaginary part, that is

$$\Im G(\mathbf{r}_1, \mathbf{r}_2, \omega) = \pi \,\text{signum}(\mu - \epsilon_i) \sum_i f_i(\mathbf{r}_1) f_i^*(\mathbf{r}_2) \delta(\omega - \epsilon_i). \tag{2.18}$$

The imaginary part of G has different sign depending on the sign of ω. We would certainly like to deal with an always positive function. Let us then define the spectral function as

$$\begin{aligned} A(\mathbf{r}_1, \mathbf{r}_2, \omega) &= \frac{1}{\pi} \,\text{signum}\,(\mu - \omega) \Im\left[G(\mathbf{r}_1, \mathbf{r}_2, \omega)\right] \\ &= \sum_i f_i(\mathbf{r}_1) f_i^*(\mathbf{r}_2) \delta(\omega - \epsilon_i). \end{aligned} \tag{2.19}$$

A is a real and positive function of ω. Numerically speaking, this could be an advantage. It carries the same amount of information as the Green's function (as there is a relation between real and imaginary parts of G). Let us see some interesting properties of the spectral function that can be of practical interest. First, there is a sum-rule; second, A brings directly the ground-state density:

$$\int_{-\infty}^{+\infty} d\omega A(\mathbf{r}_1, \mathbf{r}_2, \omega) = \delta(\mathbf{r}_1 - \mathbf{r}_2) \tag{2.20a}$$

$$\int_{-\infty}^{\mu} d\omega A(\mathbf{r}_1, \mathbf{r}_1, \omega) = n(\mathbf{r}_1). \tag{2.20b}$$

Moreover, the photoemission spectrum can approximately be calculated from the spectral function. With the assumption that the outgoing electron is decoupled from the system, the photocurrent is

$$\mathcal{J}_{\mathbf{k}}(\omega) = \sum_m |\Delta_{\mathbf{k}m}|^2 A_{mm}(E_{\mathbf{k}} - \omega) \tag{2.21}$$

where $\Delta_{\mathbf{k}n}$ is the dipole-moment operator component on a complete set of single-particle wavefunctions and A_{mm} is the m-th diagonal element of A, provided that A is diagonal on this particular set.

Still, we did not advance our knowledge of how to calculate G nor A. Now we know that several interesting properties come from the Green's function, but we still seek a method to find it. This will be unveiled in the next subsection.

2.3.2 Green's function's equation of motion and the self-energy

Starting from the equation of motion for the Heisenberg creation and annihilation field operators $\hat{\psi}^\dagger$ and $\hat{\psi}$, a hierarchy of equations of motion for the Green's function can be derived. The one-particle Green's function depends on the two-particle one:

$$\left[i\frac{\partial}{\partial t_1} - h(\mathbf{r}_1)\right] G(1,2) + i\int d3 v(1,3) G_2(1,3^+;2,3^{++}) = \delta(1,2), \tag{2.22}$$

the two-particle one on the three-particle one and so on... $h(\mathbf{r}_1)$ is the independent particle hamiltonian, which contains only the external potential. The two-particle Green's function is defined as

$$i^2 G_2(1,2;1',2') = \langle N|\mathcal{T}\left[\hat{\psi}(1)\hat{\psi}(2)\hat{\psi}^\dagger(2')\hat{\psi}^\dagger(1')\right]|N\rangle \tag{2.23}$$

Actually, equation (2.22) shows in its second term that the evolution of a particle in a solid is influenced by the Coulomb interaction, which is a two-particle interaction. This is the physical reason of why the two-particle Green's function appears. The level of complexity of the complete hyerarchy of n-particle Green's functions equations ($n = 1 \ldots N$) is the same as that of the N-body problem, just reformulated in terms of Green's functions.

Here comes the fundamental idea of many-body perturbation theory: if one is interested in one-particle properties, one only needs to know the one-particle Green's function. As a consequence, one would like to find good appoximations that allow one to re-write the two-particle Green's function in terms of one-particle ones.

In the next section we will see that is possible to reformulate the two-particle Green's function in terms of an operator Σ (operating on the one-particle Green's function) called *self-energy*, that accounts for all two-particles effects:

$$\begin{aligned} i\int d3\ v(1,3)G_2(1,3^+;2,3^{++}) = i\int d3\ v(1,3)G(3,3^+)G(1,2) + \\ -\int d3\ \Sigma(1,3)G(3,2) \end{aligned} \tag{2.24}$$

where the first term on the right-hand side is actually the Hartree term, as the electronic density n is equal to $-iG(3,3^+)$. This can be put in (2.22) and yields the so-called Dyson equation:

$$\left[i\frac{\partial}{\partial t_1} - h(\mathbf{r}_1)\right] G(1,2) - \int d3\Sigma(1,3)G(3,2) = \delta(1,2). \tag{2.25}$$

where the Hartree term is now included in $h(\mathbf{r}_1)$. The purpose of many-body perturbation theory is then to find suitable approximations for the operator Σ to reformulate it as a function of one-particle Green's function only.
Some physical insight of Σ can be given by the following pseudo-Schrödinger equation:

$$\int d\mathbf{r}_3 \left[h(\mathbf{r}_1)\delta(\mathbf{r}_1 - \mathbf{r}_3) + \Sigma(\mathbf{r}_1, \mathbf{r}_3, \epsilon_i)\right] f_i(\mathbf{r}_3) = \epsilon_i f_i(\mathbf{r}_1), \tag{2.26}$$

which is obtained by introducing Lehmann's representation of one-particle Green's function in equation (2.22), after a Fourier transform into frequency space. In this equation the self-energy acts as a complex, non-local and energy-dependent potential which includes all many-body interaction of the system. The ϵ_i are called *quasiparticle excitation energies* and are the real photoemission excitation energies of the system.

It is possible to define a non-interacting Green's function of a non-interacting particle in the common way used in many fields of physics, as the functional inverse of the Hamiltonian:

$$\left[i\frac{\partial}{\partial t_1} - h(\mathbf{r}_1)\right] G_0(1,2) = \delta(1,2). \tag{2.27}$$

This shows that we can write the non-interacting Hamiltonian in the Dyson equation (2.25) as G_0^{-1} and re-write

$$\left[G_0^{-1}(1,3) - \Sigma(1,3)\right] G(3,2) = \delta(1,2) \tag{2.28}$$

or, equivalently (and in a more elegant way as well):

$$G = G_0 + G_0 \Sigma G. \tag{2.29}$$

Again, this formula shows how Σ carries all information about many-body interactions and connects the interacting system with the non-interacting one. Still, the self-energy is an unknown operator. In the next subsection Hedin's approach will be described. This approach shows a way to calculate Σ and reveals some more of its physical meaning as well.

2.3.3 Hedin's equations

There is a little trick due to Schwinger [30] which allows one to decouple the hierarchy of Green's functions' equations, i.e. introducing a small external time-dependent perturbation of the system $U(1,2)$ which will be eventually brought to zero at the end of the derivation. Thanks to Schwinger's technique, it can be shown that:

$$\frac{\delta G(1,2)}{\delta U(3,4)} = -G_2(1,4;2,3) + G(1,2)G(4,3). \tag{2.30}$$

With this equation it is possible to write the two-particle Green's function in terms of one-particle ones (Just what we have been looking for so far!). We can then substitute G_2 in the equation of motion of the one-particle Green's function (2.22) and thus find two equivalent expressions[2] for Σ:

$$\Sigma(1,2) = -i \int d345 G(1,4) \frac{\delta G^{-1}(4,2)}{\delta U(3)} v(1^+,3) \tag{2.31a}$$

$$= i \int d345 G^{-1}(4,2) \frac{\delta G(1,4)}{\delta U(3)} v(1^+,3). \tag{2.31b}$$

Now we "only" have to calculate G with equation (2.29) and we will have the solution of our problem. We will now see how. Hedin [4, 5] introduces at first the local classical potential $V(1)$:

$$V(1) = U(1) - i \int d2 v(1,2) G(2,2^+), \tag{2.32}$$

which is the sum of the external perturbation U and the Hartree potential $V_H(1) = -i \int d2 v(1,2) G(2,2^+)$. By the functional derivative's chain rule[3] we can reformulate equation (2.31a) as

$$\Sigma(1,2) = -i \int d345 G(1,4) \frac{\delta G^{-1}(4,2)}{\delta V(5)} \frac{\delta V(5)}{\delta U(3)} v(1,3^+). \tag{2.33}$$

At this point, we can introduce the time-ordered inverse dielectric function:

$$\varepsilon^{-1}(1,2) = \frac{\delta V(1)}{\delta U(2)}, \tag{2.34}$$

and the irreducible vertex function:

$$\tilde{\Gamma}(1,2;3) = -\frac{\delta G^{-1}(1,2)}{\delta V(3)}; \tag{2.35}$$

the term "irreducible" means that the functional derivative is performed with respect to the classical local potential V and not only with respect to the external potential U. It is possible to define reducible functions differentiating with respect to U. Let us now introduce the dynamical screened Coulomb interaction:

$$W(1,2) = \int d3 v(1,3) \varepsilon^{-1}(3,2) \tag{2.36}$$

[2] For two generic functionals $G(1,2)$ and $U(1)$, $\frac{\delta G(1,2)}{\delta U(3)} = -\int d45 G(1,4) \frac{\delta G^{-1}(4,5)}{\delta U(3)} G(5,2)$

[3] For three generic functionals A,B and C with $A = A[B[C]]$, $\frac{\delta A[B[C]](1)}{\delta C(2)} = \int d3 \frac{\delta A[B](1)}{\delta B(3)} \frac{\delta B[C](3)}{\delta C(2)}$

and then re-write the self-energy as:

$$\Sigma(1,2) = i \int d34 G(1,4) W(3,1^+) \tilde{\Gamma}(4,2;3). \tag{2.37}$$

We still have to provide some tractable expressions for $\tilde{\Gamma}$ and ε^{-1}. Using the Dyson equation $G^{-1} = G_0^{-1} - V - \Sigma$, equation (2.34) is worked out with some functional analysis to give

$$\tilde{\Gamma}(1,2;3) = \delta(1,2)\delta(1,3) + \int d4567 \frac{\delta\Sigma(1,2)}{\delta G(4,5)} G(4,6) G(7,5) \tilde{\Gamma}(6,7;3). \tag{2.38}$$

Concerning ε^{-1}, we shall use the definition of V and write:

$$\varepsilon^{-1}(1,2) = \delta(1,2) + \int d3 v(1,3) \chi(3,2), \tag{2.39}$$

where

$$\chi(1,2) = -i \frac{\delta G(1,1^+)}{\delta U(2)} \tag{2.40}$$

is the reducible polarizability of the system. The irreducible polarizability can be introduced as

$$\tilde{\chi}(1,2) = -i \frac{\delta G(1,1^+)}{\delta V(2)} \tag{2.41}$$

which is related to χ by

$$\chi(1,2) = \tilde{\chi}(1,2) + \int d34 \tilde{\chi}(1,3) v(3,4) \chi(4,2). \tag{2.42}$$

Finally, $\tilde{\chi}(1,2)$ can be written as a function of G and Σ:

$$\tilde{\chi}(1,2) = -i \int d34 G(1,3) G(4,1) \tilde{\Gamma}(3,4;2). \tag{2.43}$$

We can finally write Hedin's set of five equations in five variables [4, 5]:

$$G(1,2) = G_0(1,2) + \int d34 G_0(1,3) \Sigma(3,4) G(4,2) \tag{2.44a}$$

$$\tilde{\Gamma}(1,2;3) = \delta(1,2)\delta(1,3) + \int d4567 \frac{\delta\Sigma(1,2)}{\delta G(4,5)} G(4,6) G(7,5) \tilde{\Gamma}(6,7;3) \tag{2.44b}$$

$$\tilde{\chi}(1,2) = -i \int d34 G(2,3) G(4,2) \tilde{\Gamma}(3,4;1) \tag{2.44c}$$

$$W(1,2) = v(1,2) + \int d34 v(1,3) \tilde{\chi}(3,4) W(4,2) \tag{2.44d}$$

$$\Sigma(1,2) = i \int d34 G(1,4) W(3,1^+) \tilde{\Gamma}(4,2;3) \tag{2.44e}$$

where W is written as a function of $\tilde{\chi}$ to avoid introducing the intermediate quantities ε^{-1} and χ.

In his original paper [4], Hedin mentioned that these equations can be viewed as an iterative solution of the many-body problem, but he stressed that they would be interesting if only very few iterations were actually needed (for a matter of calculation weight). Basically the calculation starts with some hypothesis on Σ and G; then $\tilde{\Gamma}$ and $\tilde{\chi}$ are evaluated. At this point W and then Σ can be calculated. Now one knows an improved Green's function G and can start again the same procedure, with the new Σ and G. This procedure can be represented by the pentagon in figure 2.1, where each corner symbolizes an unknown variable and each edge one of the five Hedin equations. The exact solution can be obtained in principle upon completion of numerous cycles of the pentagon.

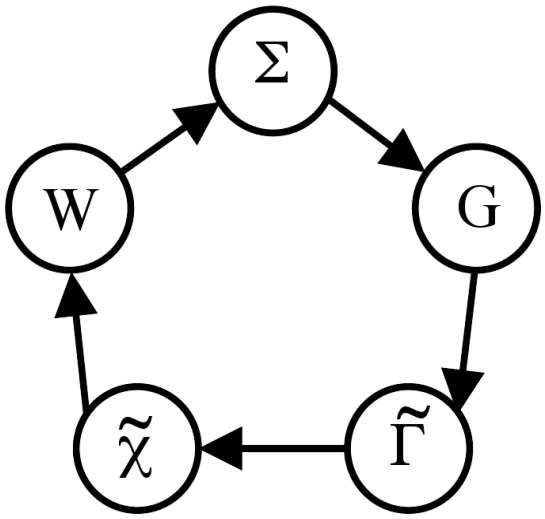

Figure 2.1: Hedin's pentagon, representing one cycle of calculation of Σ.

2.3.4 The *GW* approximation

Using W instead of v as basic interaction line is motivated by the hope that the perturbation theory will converge faster with respect to powers of W, than with respect to the powers of v. Having this hope in mind, Hedin proposed to retain only first-order contributions in W. This yields the so-called GW approximation that consists in initiating the iterative scheme with $\Sigma = 0$ in the vertex equation:

$$\tilde{\Gamma}(1,2;3) = \delta(1,2)\delta(1,3). \tag{2.45}$$

The resulting self-energy is just

$$\Sigma(1,2) = iG(1,2)W(2,1^+), \tag{2.46}$$

that gives its name to the approximation. The corresponding irreducible polarizability reads

$$\tilde{\chi}(1,2) = -iG(1,2)G(2,1) = \chi_0(1,2) \tag{2.47}$$

which is the definition of the independent-particle (or RPA) polarizability χ_0.

The standard *GW* approach that permits to calculate the photoemission excitation energies starts from the comparison of the quasiparticle equation (2.22) and the Kohn-Sham equation (2.6). The exchange-correlation potential and the self-energy act both as a potential, with Σ being much more complicated than v_{xc}^{KS}. If one supposes that the Kohn-Sham orbitals are a decent approximation of the quasiparticles, it is reasonable to consider $\Sigma - v_{\text{xc}}^{KS}$ as a first-order perturbation to the Kohn-Sham Hamiltonian. The GW energies are hence most often calculated as first-order corrections of the Kohn-Sham energies by this formula:

$$\epsilon_{\mathbf{k}_i i}^{GW} = \epsilon_{\mathbf{k}_i i}^{KS} + Z\langle\phi_{\mathbf{k}_i i}|\Sigma(\epsilon_{\mathbf{k}_i i}^{KS}) - v_{\text{xc}}^{KS}|\phi_{\mathbf{k}_i i}\rangle, \tag{2.48}$$

where

$$Z = \frac{1}{1 - \frac{\partial\Sigma}{\partial\epsilon}\Big|_{\epsilon_{\mathbf{k}_i i}^{KS}}}. \tag{2.49}$$

Moreover, the Σ dependence on $\epsilon_{\mathbf{k}_i i}^{GW}$ is approximated by linearizing Σ in the neighbourhood of the Kohn-Sham energies $\epsilon_{\mathbf{k}_i i}^{KS}$. The Z factor comes from the linearization. The self-energy is also constructed with Kohn-Sham LDA wavefunctions via the Green's function G and the RPA screening W. This procedure is known as *one-shot GW*, G_0W_0 or *perturbative GW* and has been proved to be very successful in predicting photoemission gaps of various compounds. Throughout the thesis I will refer to this method also as *GW+LDA*.

2.3.5 Hartree-Fock self energy

The Hartree-Fock approximation can be re-introduced at this point, writing the self-energy as

$$\begin{aligned}\Sigma_x(1,2) &= i\,v(1^+,2)G(1,2) \\ &= -\,v(\mathrm{r}_1,\mathrm{r}_2)\gamma(\mathrm{r}_1,\mathrm{r}_2) = -\sum_{occ}\phi_i(\mathrm{r}_1)\phi_i^*(\mathrm{r}_2)v(\mathrm{r}_1,\mathrm{r}_2).\end{aligned} \tag{2.50}$$

$\Sigma_x(1,2)$ is the Fock exchange operator, or Hartree-Fock self-energy. $\gamma(\mathrm{r}_1,\mathrm{r}_2)$ is the density matrix. The Fock operator can be derived from GW self-energy, supposing that $\varepsilon^{-1} = 1$. The direct consequence is that the dynamical screened Coulomb

interaction is replaced by the bare static Coulomb interaction. The physical meaning is that within this approximation the system is not allowed to relax after the addition or removal of an electron, following Koopmans' theorem [6].

2.3.6 Plasmon-pole model

The calculation of the self-energy in *GW* involves a convolution of *G* and *W* in the frequency domain. This part of the calculation is very time-consuming. In fact, the matrix $\varepsilon^{-1}_{\mathbf{GG'}}(\mathbf{q},\omega)$ must be calculated for different values of $\mathbf{q}$ in the Brillouin zone, for all values of ω.[4] Since one is interested only in the value of the integral, it is acceptable to approximate the integrand to a simple form. It has been proposed to model the dependence on ω of the matrix $\varepsilon^{-1}_{\mathbf{GG'}}(\mathbf{q},\omega)$ by a single plasmon-pole model [31]:

$$\varepsilon^{-1}_{\mathbf{GG'}}(\mathbf{q},\omega) = \delta_{\mathbf{GG'}} + \frac{\Omega^2_{\mathbf{GG'}}(\mathbf{q})}{\omega^2 - (\tilde{\omega}(\mathbf{q}) - i\eta)^2} \tag{2.51}$$

where $\Omega^2_{\mathbf{GG'}}(\mathbf{q})$ and $\tilde{\omega}(\mathbf{q})$ are the two parameters of the model. The dielectric function is here approximated as a single-peak structure. The peak is located on the classical *plasmon frequency* ω_p. This model allows us to evaluate ε^{-1} everywhere in the complex plane, once the two parameters are fit. To this purpose, two constraints are needed. The ABINIT *GW* code [32, 33] chooses two frequencies where the RPA ε^{-1} is actually computed: $\omega = 0$ and $\omega \sim i\omega_p$. The use of a plasmon-pole model not only reduces the calculation of $\varepsilon^{-1}(\omega)$ (as only two frequencies are required), but also permits an analytic calculation of the frequency integral in equation (2.46).[5] The value of 24 eV for the plasmon frequency ω_p has been taken from experimental data by Aryasetiawan *et al.* [17].

2.3.7 COHSEX approximation for the self-energy

The practical application of the *GW* approximation is the perturbative approach described above. This approach relies on the approximation that considers the Kohn-Sham orbitals and energies to be quite close to the real wavefunctions. This approximation does not have a theoretical basis, but it is grounded on practice application of the method on model and realistic systems. However, there are some general known limits of Kohn-Sham LDA. Namely, the energy-gap is always smaller than the real one. This will generally provide a larger screening than the actual one and cause an underestimation of the band-gap in *GW* as well. The easiest solution is to iterate a perturbative GW calculation updating the Kohn-Sham

[4] The inverse dielectric function is defined here in reciprocal space on the **G** vectors of the plane wave basis and in frequency space.

[5] Equation (2.46) is defined in real space. A Fourier transform is necessary to write it in the frequency domain.

eigenvalues with the *GW* ones, until the energies do not change anymore. This approach is called *energy-only* self-consistency and still relies on the K-S wavefunctions as approximation of the quasiparticle wavefunctions. But in the worst case, the Kohn-Sham wavefunctions appears to be not adequate at all to describe the electronic system. In this case it is necessary to calculate new wavefunctions. The straightforward way to do it is to diagonalize the quasiparticle equation 2.26 and iterate the procedure until self-consistency in energies and wavefunctions is reached. This can be quite a time-consuming approach, since the self-energy is a non-hermitian, non-local, complex and energy-dependent operator. In the case of a self-consistent calculation Σ is diagonalized at each self-consistent step. To this purpose, one needs an approximation to make Σ hermitian. The COHSEX approximation for the self-energy, first proposed by Hedin as an affordable approximation of *GW* [4], is not only hermitian, but also static and requires a sum only over the occupied states, being hence much more affordable from a computational point of view. Σ^{COHSEX} is the sum of two terms. The first is the following:

$$\Sigma^{\text{SEX}}(\mathbf{r}_2, \mathbf{r}_1) = -\sum_i \theta(\mu - \epsilon_i) f_i(\mathbf{r}_1) f_i^*(\mathbf{r}_2) W(\mathbf{r}_2, \mathbf{r}_1, \omega = 0) \tag{2.52}$$

that is the *screened exchange* part (SEX). This formula is almost identical to equation (2.50), except that here the static screened Coulomb interaction has taken the place of the bare Coulomb interaction. This term should take into account correctly the fermionic nature of electrons and at the same time the fact of being in a polarizable medium, damping the exchange interaction. The sum only over occupied states ensures a limited computational effort, whereas in the *GW* self-energy one has to sum over all the empty states as well. Being static, the calculation of W requires to calculate ε^{-1} at $\omega = 0$ only. The second term is

$$\Sigma^{\text{COH}}(\mathbf{r}_2, \mathbf{r}_1) = \frac{1}{2}\delta(\mathbf{r}_1 - \mathbf{r}_2) W_p(\mathbf{r}_2, \mathbf{r}_1, \omega = 0), \tag{2.53}$$

where $W_p = W - v$ is the *polarizable part* of W. This second term is called the *Coulomb hole contribution* to the self-energy (COH). It is static and local in space. This latter term represents the energy shift due to the polarization of the system induced by an added hole or electron. The particle is approximated by a classical point charge.

The COHSEX approximation for the self-energy is quite crude, but it gives a quite immediate physical insight, so that it is clear what effects are included in the self-energy (exchange, static screening and polarizability) and what are missing (dynamical correlation, e.g. satellites). Moreover, it is computationally much more affordable than standard *GW*. This approximation is known to be a reliable approach for self consistent calculations, whose pourpose is to calculate new wavefunctions [34–36]. The dynamical effects neglected in Σ^{COHSEX} are normally included in the calculation by a last perturbative *GW* step on top of the converged

COHSEX band structure. Self-consistent COHSEX is actually a way to calculate proper quasiparticle wavefunctions that can ben used as a reliable starting-point for perturbative *GW*.

2.3.8 Self-energy beyond *GW*: vertex corrections

I have listed above the *GW* approximation and other simpler approximations for the self-energy, such as Hartree-Fock and COHSEX. But what if one wanted to adopt an approximation *better* than *GW*? In this case one has to take a look at Hedin's equations. There, the exact form of the self-energy is

$$\Sigma(1,2) = i \int d34 G(1,4) W(3,1^+) \tilde{\Gamma}(4,2;3) \tag{2.54}$$

where $\tilde{\Gamma}(4,2;3)$ is the irreducible vertex function, as taken in equations (2.44). In standard *GW* approach to solve Hedin's equations, the vertex function is taken as $\delta(4,2)\delta(4,3)$, i.e. $\Sigma^0 = 0$ is taken as the starting point of the one-step perturbative approach. In this case one says that vertex corrections are neglected. This is a quite drastic approximation, but it has been proven to be a fair one in practical applications. Del Sole *et al.* [37] tried to improve the *GW* approximation with an approximate vertex correction. In their article they start the perturbative calculation approximating Σ with the LDA exchange-correlation potential $V_{\text{xc}}^{\text{LDA}}(\mathbf{r})$. The starting self-energy then becomes

$$\Sigma^0(1,2) = \delta(1,2) V_{\text{xc}}(1). \tag{2.55}$$

This starting point produces, in the first iteration of Hedin's equations, a self-energy of the form $\Sigma = G\tilde{W}$, where $\tilde{W}$ is an effective dynamical screened Coulomb interaction. The difference between W and $\tilde{W}$ is that the in the latter case the screening is described by the so-called electron–test-charge dielectric function. While the RPA ε^{-1} used in *GW* is the classical screening between two classical charges, in this case the screening used to calculate $\tilde{W}$ describes the effect of an additional charge on the potential felt by an electron. The essential difference is that in W, the induced charge generates only a Coulomb potential, while in $\tilde{W}$ the induced charge also generates an exchange-correlation potential.

This is called the $GW\Gamma$ approximation, from the complete form of Σ in Hedin's equations. This approach has the advantage to go beyond the *GW* approximation while retaining the same computational cost. The actual need for vertex corrections is still under debate, since it is not clear if and how much they can improve the *GW* results. Also, it might be necessary to adopt different approximations for $\tilde{\Gamma}$. Possible vertex corrections different from the one presented above, are discussed in References Ref. [34].

2.4 The concept of quasiparticle in photoemission spectroscopy

I have extensively used in the previous sections terms like *quasiparticle* and *quasiparticle energies*. The term *quasiparticle* stands in opposition to the term *independent particle*. We refer to an independent particle when the Hamiltonian of the system is a single-particle Hamiltonian which takes into account the presence of other electrons by an effective external potential. In this picture the electrons are independent particles, whose behaviour is slightly affected by their surrounding. This is e.g. the case of the Bloch picture for solids, where electrons are travelling waves in a periodic external potential. In a photoemission experiment, an independent photoelectron, after being excited by a photon, leaves the solid without any interaction with the system producing a spectral peak which is a delta peak at the exact energy of the electron in the solid.

Even though the independent particle approximation has made possible the developement of solid-state physics and has proven its possible application in a variety of materials, it is a quite drastic approximation. In its complete treatment, the electronic structure problem is a *many-body* problem, i.e. each electron is constantly interacting with a number of other electrons in the system that modify its behaviour accordingly. The Coulomb interaction between the electrons is thus *screened* by themselves, depending on their reciprocal arrangement in the system. In this picture, a precise definition of a single particle can be difficult. Nevertheless, photoemission spectra can give some clues, in fact photoemission spectra can exibit structures that are very single-particle-like, e.g. strong peaks very similar to delta peaks. But sometimes photoemission spectra can have a very different shape, very broadened and without clear peaks at all. The broadened shapes are called *satellites* and are often the expression of collective excitations of the system. One can have of course both kinds of behaviour. These two very different kinds of features in photoemission spectra mark the fact that electrons can show a very different behaviour depending on the environment they are in.

A *quasiparticle* is an electron surrounded by the screened interaction with the other particles in the system. In this picture, the electron travels in the solid surrounded by what can be called a *polarization cloud*, that depends on the screening and consequently on the polarizability of the system. This "surrounding-dependent" particle is the link between the single-particle world and the many-body world. In fact, quasiparticles can have a behaviour quite similar to independent particles. In the case of quasiparticles, one can still speak of quasiparticles band-structures and energies, when the system is not too *correlated*. *Correlation* is by definition every effect one takes into account beyond the Hartree-Fock approximation, which only takes into account the fermionic nature of electrons. In this

case the photoemission energies are delta peaks by construction.

When the single-particle description breaks down completely one talks about *strongly correlated* materials. In this materials the photoemission spectrum shows many-body features like satellites and loses any recognizable single-particle feature. Strongly correlated materials have been and are still under the attention of researchers because of the difficulty to explain the physical processes underneath their properties. This is e.g. the case of NiO, that shows both weakly and strongly correlated properties.

Quasiparticles energies are what is measured in photoemission. Hence, an adequate theoretical description is needed to calculate the spectrum. In literature photoemission spectra are often compared to Kohn-Sham–LDA or independent-particle Densities Of States. This arbitrary approach has nevertheless been used extensively. The reason for this sort of "abuse" of a ground-state theory like DFT is to be found in the overall good agreement between Kohn-Sham bands and DOSes and experimental data of many materials. Also, Kohn-Sham LDA's computational cost is very low. But a proper description of the photoemission process needs an excited-state theory, such as many-body perturbation theory, where the Green's function describes precisely the process of creating a hole (or adding an electron) and the quasiparticle excitation energies come hence naturally from the theory. Quasiparticles have a finite lifetime and can exibit many-body features like satellites. The *GW* approximation is an affordable way to get a correct physical description of the photoemission process that can be compared to experimental data.

Chapter 3

Exchange and spin interactions in the electronic structure of NiO

In this chapter the ground-state electronic structure of NiO will be first analyzed by means of Density-Functional Theory, calculating the Kohn-Sham band structure and the density of states. The experimental structural parameters have been taken into account. Secondly, the Hartree-Fock method will be applied to the system to stress out the role played by exchange in this material, especially for what concerns the paramagnetic phase. The whole procedure will be carried out for both the paramagnetic and the anti-ferromagnetic case, i.e. including the spin explicitly in the calculation for the latter case. This definition will be always implicit in the following.

3.1 NiO: a strongly-correlated material

Nickel oxide is an insulator which undergoes an anti-ferromagnetic–paramagnetic phase transition at 523-525 K [7, 8]. The magnetic transition temperature T_N is called the Néel temperature. There is also a slight change in the crystal structure, which passes from a rhombohedral to a rocksalt structure [9] (i.e. like NaCl). The photoemission energy-gap of this material is 4.3 eV [7]. There is no change in the value of the gap while passing above the Néel temperature.

Figure 3.1 shows the experimental photoemission spectrum published by Sawatzky and Allen [7] in 1984. It is a combined x-ray–photoemission (XPS) and bremsstrahlung-isocromat-spectroscopy (BIS) (i.e. inverse photoemission) measurement. The valence bands exibit a strong peak just below the Fermi level which, in a band-structure description, is supposed to originate from nickel *d* bands. Lower in energies (at about 4 eV) there are other peaks which come from *p* bands of oxygen, that are more evident in the 66 eV XPS data. At about 8 and 11 eV there

are structures that one cannnot classify in a single-particle band-structure picture. These are nickel oxide's satellites. The inverse photoemission data show a strong peak just above the energy-gap. This peak is supposed to originate from nickel e_g *d* bands. The experimental resolution of the spectrum is reported to be 0.6 eV.

The origin of the energy-gap of NiO is still under debate. Before the discovery of antiferromagnetism, it was pointed out that, according to the Wilson theory of metals and insulators (which describes materials in terms of Bloch's states and bands), nickel oxide should be a metal — whereas it is a transparent insulator. The e_g bands were predicted to be crossing the Fermi level and hence to be half-filled. Slater [38] showed in 1951 that the antiferromagnetic sublattice in NiO could split the e_g bands into two bands with two electrons per atom in each, and thus explain its insulating properties, but pointed out that there is no marked increase in the conductivity when the temperature is raised above the Néel temperature, even though a band structure description would predict a metal in the latter case. Moreover, conductivity measurements on pure NiO are hard, because the resistivity is high and measurements are very sensitive to surface conduction [10]. Another difficulty in doing measurements on NiO is that at the Néel temperature it is sublimating. It is thus necessary to perform any measurement as quickly as possible, to avoid sensitive changes in the material [8]. In NiO a metal-insulator transition has been observed under very high pressure (2.5 Mbar): the conductivity at room temperature drops abruptly by about 10^6. Nothing was determined regarding the temperature dependence of the conductivity, or the change of volume [10].

Nickel oxide was first taken by Mott as the paradigmatic material for *Mott-Hubbard insulators*, described in terms of the Hubbard model [39]. The Hubbard model describes a solid as a regular lattice of 1-band sites and takes into account both the itinerant and the localized nature of electrons. Here is the Hubbard Hamiltonian, in the formalism of second quantization:

$$\hat{H} = -t \sum_{\langle ij \rangle \sigma} (\hat{c}^{\dagger}_{i\sigma} \hat{c}_{j\sigma} + h.c.) + U \sum_{i} \hat{n}_{i\uparrow} \hat{n}_{i\downarrow}. \tag{3.1}$$

Given a hopping (i.e. site transfer) probability t, the key parameter is U, which is the magnitude of the on-site interaction, i.e. the energy that must be paid to put two electrons on the same lattice site. The Pauli principle must be obeyed, hence two electrons can be on the same site only if they have opposite spins. Depending on the U/t ratio, the system can be either a metal or an insulator. Its later developements like Dinamical Mean Filed Theory (DMFT) have claimed to describe properly a variety of materials. Mott pointed out that Slater's description was valid for the ground-state of the system, i.e. at 0 K, but equivalent to his description, that was moreover valid at all temperatures and independent on the spin configuration. Some authors [7] describe nickel oxide not as a *Mott-Hubbard* insulator in the simplest sense, where the interaction is between *d* electrons. but as a

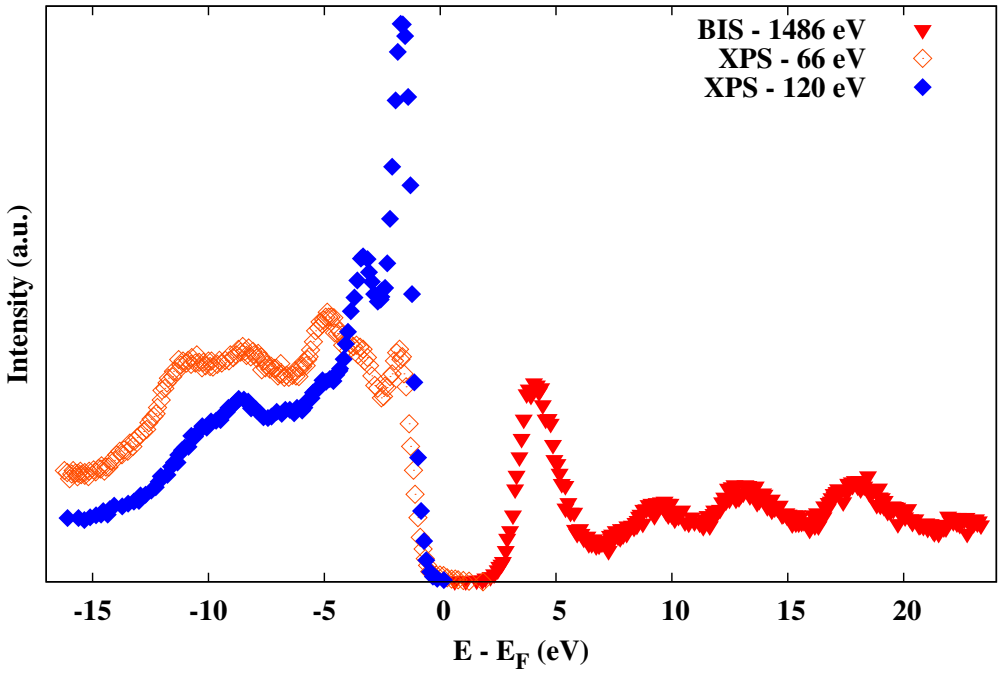

Figure 3.1: Direct (XPS) and inverse (BIS) measured photoemission spectrum of nickel oxide. For the direct photoemission part two values of the photon energy are shown. The value of the gap is 4.3 eV. The uncertainty on the measurement is 0.6 eV [7].

charge-transfer insulator, where the oxygen *p* electrons participate to the Hubbard interaction. The applicability of this kind of models to systems like NiO is justified by the very localized nature of the $3d$ electrons which determines a strong *on-site* Coulomb interaction. This characteristic, common to several transition-metal compounds described by means of the Mott-Hubbard model, has often caused some misleading, confusing *strongly correlated* materials with materials where the Mott-Hubbard model is applicable. Instead, strong correlation should be more largely intended as every effect that prevents (partly or at all) a description of a system in a single-particle picture, i.e. when many-body effects have a non-negligible contribution.

Local Spin-Density Approximation

The anti-ferromagnetic structure of NiO, which is the stable configuration under 523 K, requires the explicit treatment of the spin in the calculation. This requirement is fulfilled by the extension of LDA to the spin domain, which is normally referred to as the *Local Spin Density Approximation* (LSD or LSDA). The crystal lattice is slightly different from the paramagnetic one, in fact it is a rhombohedral (or, equivalently, trigonal) structure. The description of the anti-ferromagnetic structure requires to have two nickel atoms able to have opposite spin orientation. Thus, the unit cell needs to be doubled. The unit cell for the anti-ferromagnetic configuration contains then two nickel atoms and two oxigen atoms respectively. This trick, originally due to Slater, may seem a bit arbitrary, but actually it is just a way to permit the system to propagate in the spin degree of freedom. The inclusion of the spin variable in the calculation would not be necessary in principle, since the Hohenberg-Kohn theorem states that every ground-state variable (such as the magnetization) can be calculated as a functional of the density only. In the practical implementation of DFT, one needs to define the Kohn-Sham system to make actual calculations, since the exact functional is unknown. Similarly, it appears easier to extend the theory adding the spin variable to the Kohn-Sham system, instead of looking for an unknown functional of the density, since this way one can build an approximate functional in a feasible way [40].

For non-magnetic materials the explicit treatment of spin brings to exactly the same results than a calculation without spin, pointing out the validity of a simpler approach that assumes *a priori* the spin degeneracy. This approach has a fall back on the computational weight of the calculation. the number of bands multiplies by four, since the unit cell is double and there is one electron per band (i.e. half the number of electrons per band with respect to the LDA case) so that we have twice the number of bands per atom.

3.2 Lattice and magnetic structure

The unit cell of nickel oxide contains one nickel atom and one oxygen atom. I will briefly present the structural parameters that have been used in my work to modelize the lattice and that have been used for all calculation in DFT, Hartree-Fock and *GW* for the paramagnetic and the anti-ferromagnetic phases.

Rocksalt structure – Paramagnetic phase The rocksalt lattice structure is the the combination of two FCC lattices, shifted by a half of the lattice constant along one axis direction (e.g. [100]). It is the same structure of NaCl. The lattice constant is a=4.19056 Å at 550 K. The space group is $Fm\bar{3}m$. These values have been determined by experiment and are taken from the literature [9]. The unit cell contains one atom of nickel and one atom of oxygen. A portion of the rocksalt lattice is shown in Figure 3.2. The Brillouin zone is the FCC Brillouin zone, i.e. a truncated octahedron. The FCC Brillouin zone is displayed in Figure 3.3. See [41] for an extensive treatment of direct and reciprocal lattices.

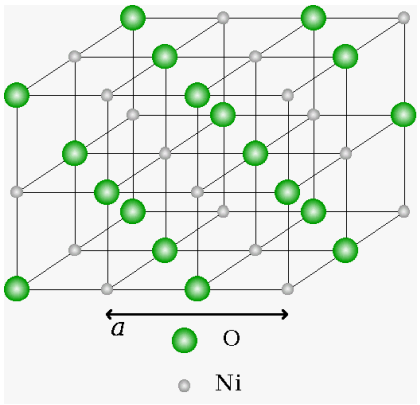

Figure 3.2: A portion of the rocksalt lattice structure of NiO. There are two FCC sublattices for the two atomic species. The lattice constant at 550 K is *a*=4.19056 Å, i.e. twice the Ni-O distance. The unit cell contains two atoms: one nickel and one oxygen.

Rhombohedral structure – Anti-ferromagnetic phase The transition from the paramagnetic to the the anti-ferromagnetic state is accompanied by a rhombohedral distorsion with a contraction along the [111] direction of the cubic unit cell. The resulting crystallographic symmmetry is trigonal. The space group is $R\bar{3}m$. A rhombohedral lattice is defined by three unit vectors of the same length and with a reciprocal orientation given by three angles of the same value. At 10 K,

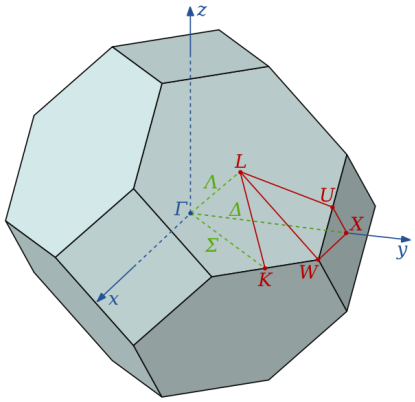

Figure 3.3: Brillouin zone for the rocksalt lattice structure of NiO. It is a truncated octahedron. The high-symmetry points are shown. Among them: Γ (000), X (100), K (110) and L (111).

the rhombohedral cell parameters are a=2.9490 Å and α=60.087° [9]. The unit cell is displayed in Figure 3.4. The spins are ferromagnetically disposed on the same (111) plane, but the planes alternate their orientation along the [111] direction, thus arranging in a AFII configuration. The description of the anti-ferromagnetic structure imposes to double the unit cell, so as to include two nickel atoms where the spin has the possibility to arrange in the proper way. Thus, the unit cell contains two nickel atoms and two oxygen atoms. The rhombohedral Brillouin zone is displayed in Figure 3.5 with the high symmetry points. In Chapter A I briefly explain how to get the coordinates of high-symmetry points in the Brillouin zone of the rhombohedral lattice.

3.3 Pseudopotentials

To represent the electronic wavefunctions I will make use of pseudopotentials and a plane wave basis, that is the most natural choice since I am treating a periodic system. A pseudopotential is an effective potential constructed to replace the atomic all-electron potential such that core states are eliminated and the valence electrons are described by nodeless pseudo-wavefunctions. The practical reason for a need of a pseudopotential is that it permits to treat explicitly (i.e. to include in the calculation) a much smaller number of electrons than the actual one and it permits to lower the plane waves basis energy cutoff — that in principle is infinite — thus reducing greatly the weight of the calculation. The physical reason that justifies the pseudopotential approximation and makes it most of the time valid is that only the

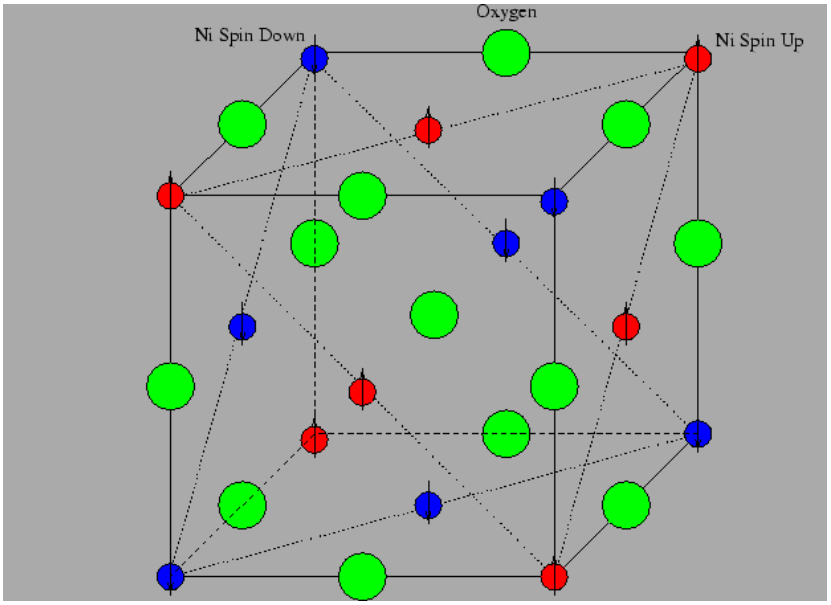

Figure 3.4: Conventional magnetic unit cell for the rhombohedral lattice structure of NiO. It is very close to a rocksalt, but actually the structure is slightly stretched along the [111] direction. It is easy to see the type-II anti-ferromagnetic configuration of nickel atoms: they are arranged on stacks of [111] planes where the spin orientation is alternatively up and down.

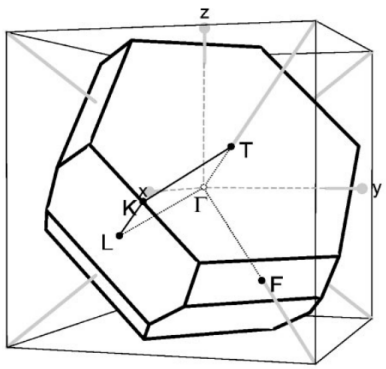

Figure 3.5: Brillouin zone for the rhombohedral lattice of NiO. The high-symmetry points are shown. Among them: Γ (000), L (100), F (110) and T (111).

electrons in the outer shell usually contribute to the chemical and physical properties of a compound. These are the so-called *valence* electrons. The "deeper" electrons (i.e. lower in energies), which fill the inner electronic shells and are usually referred to as the *core* electrons, do not normally change their behaviour appreciably when changing the ion's enviroment. In fact, the energy separation of the highest core electrons from the lowest valence electron is usually on the order of 100 eVs. The pseudopotential is therefore an effective potential which mimics the core electrons. The form of the pseudopotential is based on the atomic configuration of the core electrons. Another advantage of using pseudopotential is the fact that the valence wavefunctions do not have nodes by construction and this is a very important feature since we are using a basis of plane waves to describe the wavefunctions.

The success of the pseudopotential approximation is also validated by years of experience of many researchers who have generated and tested pseudopotentials for a variety of elements. There is a vast collection of "recipes" that describe how to generate a pseudopotential. For my work I used Trouiller-Martins [42] type pseudopotentials in a Kleinman-Bylander [43] separable form. They are generated using the fhi98PP [44] code. These are norm-conserving pseudopotentials.

In the case of NiO (and in general in the case of a transition metal oxide) there is a further detail to consider. The previous core-valence distinction is not enough. In fact, while the argument of the energy separation remains valid, there is an issue about the spatial separation of the orbitals, that influences directly the exchange part of the self-energy. If we take a look at the radial wavefunctions of atomic nickel (Figure 3.6), we can clearly see how the valence electron (i.e. *3d*) are spatially overlapped with the *3s* and *3p* orbitals. It is handy to define the *semi-core* electrons as those electrons that are in the outermost-but-one shell. It appears necessary to include in the calculation (i.e. to treat explicitly) also the semi-core electrons, since the spatial proximity to the valence ones breaks down the ansatz of semi-core and valence being separated. This becomes crucial in *GW* calculations. In principle the exchange part of the self-energy is built with the contribution of all the occupied states of the system. If they overlap with the valence states, the semi-core states cannot be evaluated simply as a Kohn-Sham LDA potential, but need to be included explicitly to construct the Σ_x operator, since the correct expression of the exchange operator is determined by the spatial overlap between wavefunctions. The validity of the inclusion the semi-core electrons is also supported by previous works on transition metal oxides like Cu_2O [34] and VO_2 [35].

The generation of a pseudopotential is carried out in several steps. First, it is necessary to choose which are the core, semi-core (if any) and valence electrons. Then, a cut-off radius must be chosen for each angular channel, on which the pseudopotential will be developed. The pseudopotential is generated by performing an all-electron scalar-relativistic calculation of the atomic configuration. The pseudo-

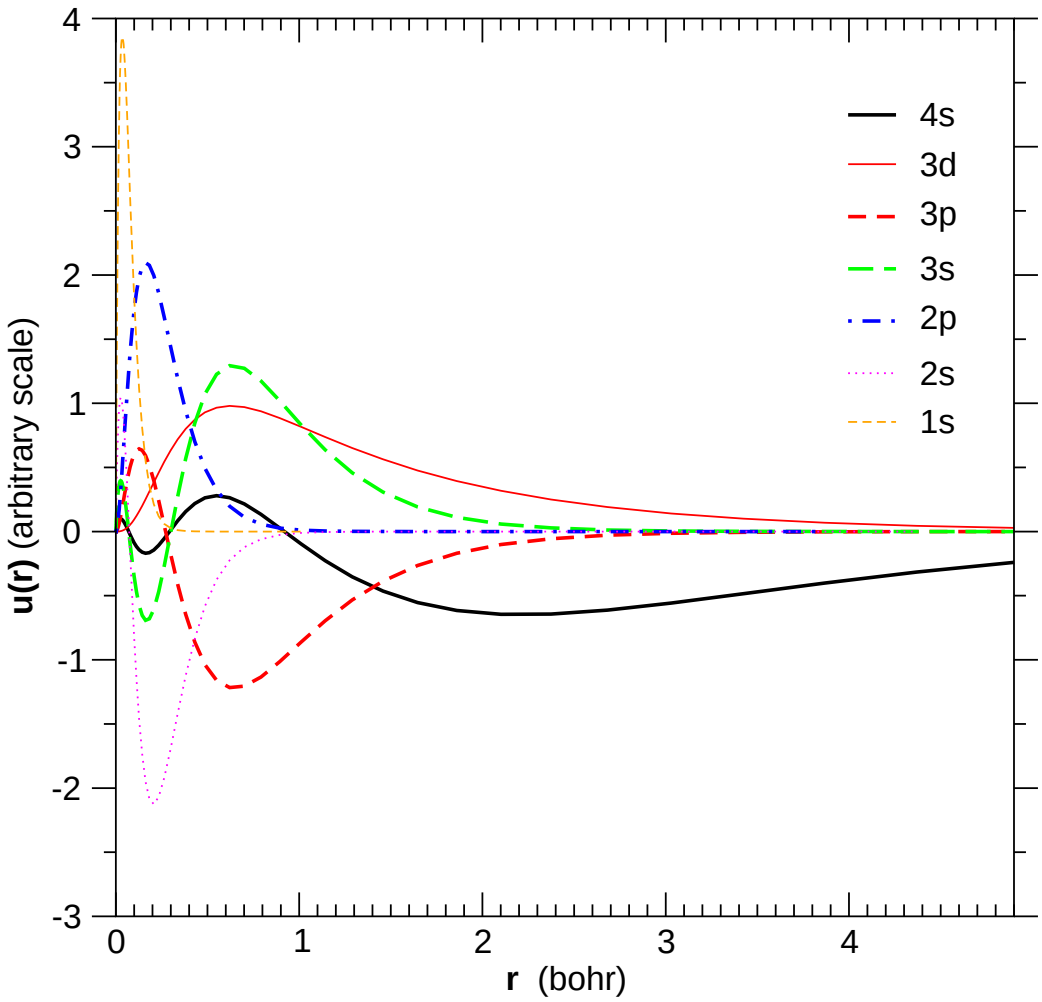

Figure 3.6: Atomic radial wavefunctions of Ni. It appears clearly how the $3s$ and $3p$ (semi-core) wavefunctions have their maximum in the same region as the $3d$ (valence) ones.

wavefunctions and potential are constructed thanks to the all-electron solution.

The oxygen electronic configuration is $1s^2 2s^2 2p^4$. In this case I took a pre-generated pseudopotential already well-tested at the *Laboratoire des Solides Irradiés* on other transition metal oxides [34, 35]. The core configuration is $1s^2$ while the valence is $2s^2 2p^4$. For the Ni atom we must take into account the semi-core states. The configuration will then be as follows. Core electrons: $1s^2 2s^2 2p^6$, semi-core electrons: $3s^2 3p^6$, valence electrons: $3d^8 4s^2$. The cut-off radius r_c for the s channel is 0.895 bohr, while for the p and d channels it is 1.087 bohr. Outside the cut-off radius the all-electron wavefunctions and the pseudo-wavefunctions must coincide, as it can be seen in Figure 3.7.

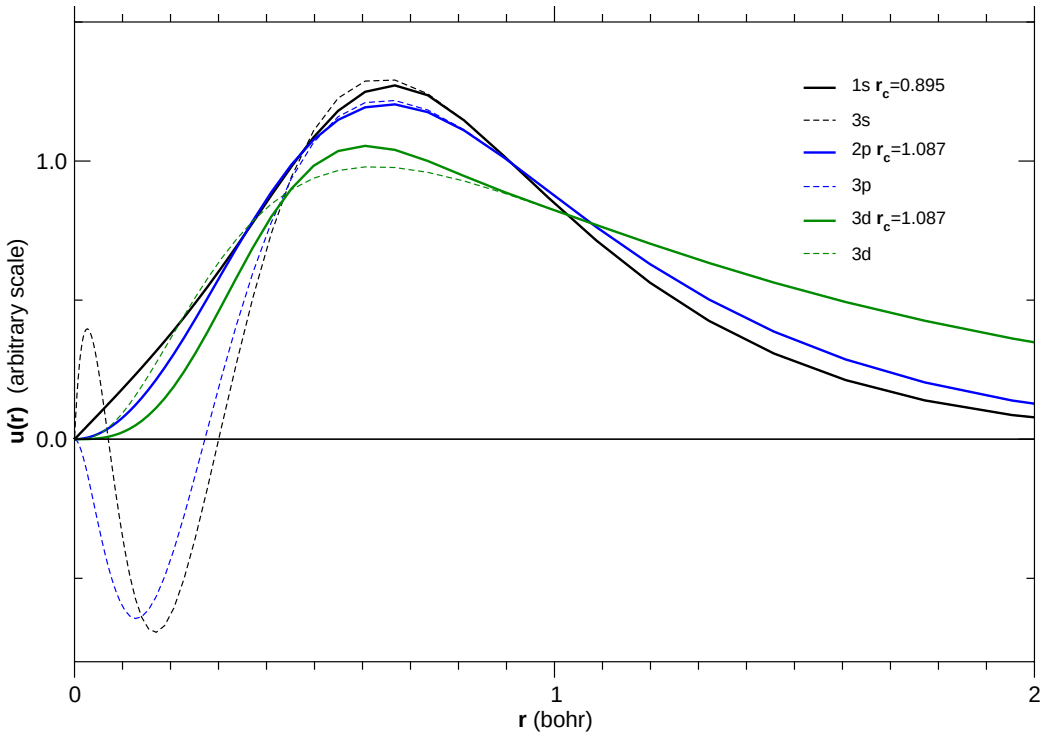

Figure 3.7: Comparison of the radial wavefunctions of Ni and their pseudo-counterparts. For each channel the cut-off radius is written. The pseudo-wavefunctions do not have nodes and coincide with the all-electron ones beyond r_c by construction.

3.4 The Ground State

The ground-state calculations are performed in the framework of the Local Density Approximation (LDA) of Density-Functional Theory, with the explicit calculation of the spin when needed (LSDA), i.e. for the anti-ferromagnetic phase. All DFT calculations have been performed with the ABINIT package. ABINIT is a software package whose main program allows one to find the total energy, charge density and electronic structure of systems made of electrons and nuclei (molecules and periodic solids) within Density-Functional Theory (DFT), using pseudopotentials and a plane wave basis. In ABINIT neutral excited states can be also computed within the Time-Dependent Density-Functional Theory (for molecules) while electron addition and removal energies within Many-Body Perturbation Theory (GW approximation). Before calculating the band structure, there is a number of parameters which need to be tuned and converged. These parameters are the kinetic energy cutoff, which has been fixed at 115 Ha, the smearing parameter (only in the case of metallic systems), which has been fixed at 0.01 Ha, and the number of k-points in the Brillouin zone, which depends on the unit cell in the direct space. For the paramagnetic phase 28 k points have been used in the irreducible Brillouin zone (6x6x6 Monkhorst-Pack grid [45]). For the anti-ferromagnetic phase (i.e. treating the spin) 42 k points have been used (6x6x4 Monkhorst-Pack grid).

Paramagnetic phase The Kohn-Sham system of the paramagnetic phase of nickel oxide, as expected, is metallic. Figure 3.8 shows how the valence bands cross the Fermi level. Following the work by Terakura *et al.* [11, 12], one can separate the bands in different contributions from the ions of the crystal. The group of bands around the Fermi level are the *d* band coming from nickel ions. Namely, the two bands crossing the Fermi level are the e_g bands, which is a notations that comes from the group theory representation of the atomic orbitals. Under the Ni *d* bands there are the *p* bands of the oxygen ions. they are well separated from the Ni *d* bands, in fact there is a small energy-gap (0.5 eV) dividing them. Above the Fermi level, the Ni *s* and O *p* bands form the upper conduction bands, separated by a small gap from the *d* bands. The density of states (Figure 3.9) exploits even better the metallic behaviour of nickel oxide in LDA. From left to right, one can distinguish the different types of bands explained above: the oxigen *p*, the nickel *d* (crossing the Fermi level) and the other conduction bands.

Anti-ferromagnetic phase The analysis of the Kohn-Sham system from the LSDA calculation on nickel oxide shows that in this case the material has a gap of 0.7 eV. Even though it is much smaller than the actual one (4.3 eV), this calcu-

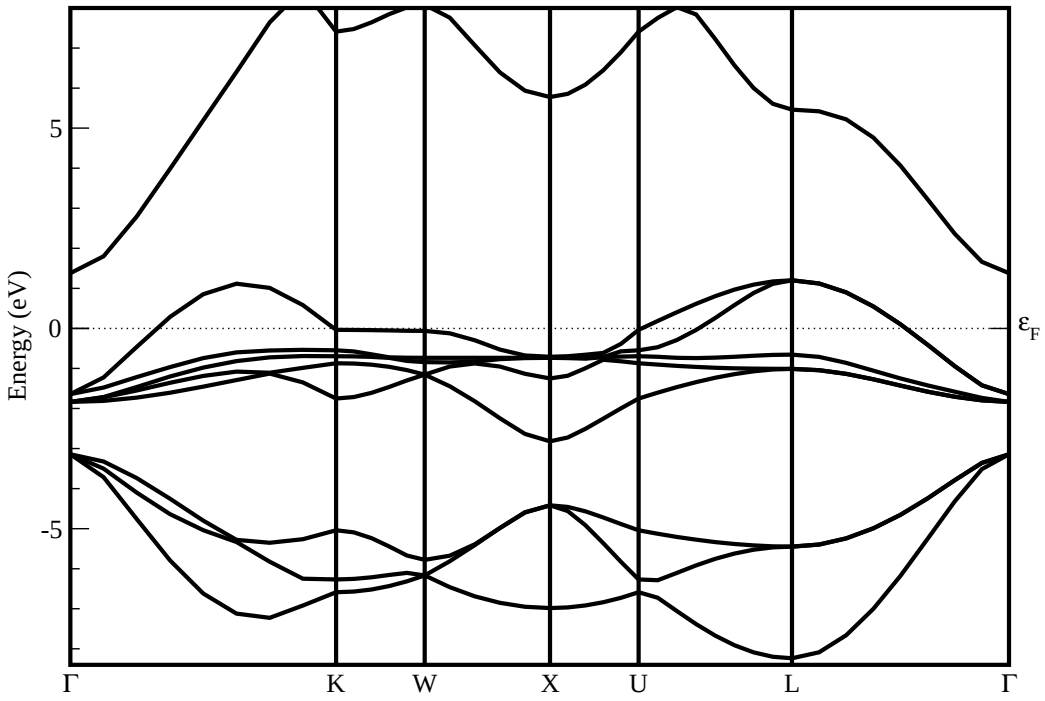

Figure 3.8: Kohn-Sham band structure of nickel oxide obtained with an LDA calculation. The crystal structure is rock-salt (NaCl-like). The special points are characteristic of the FCC Brillouin zone. The Fermi level ε_F is set at 0 eV.

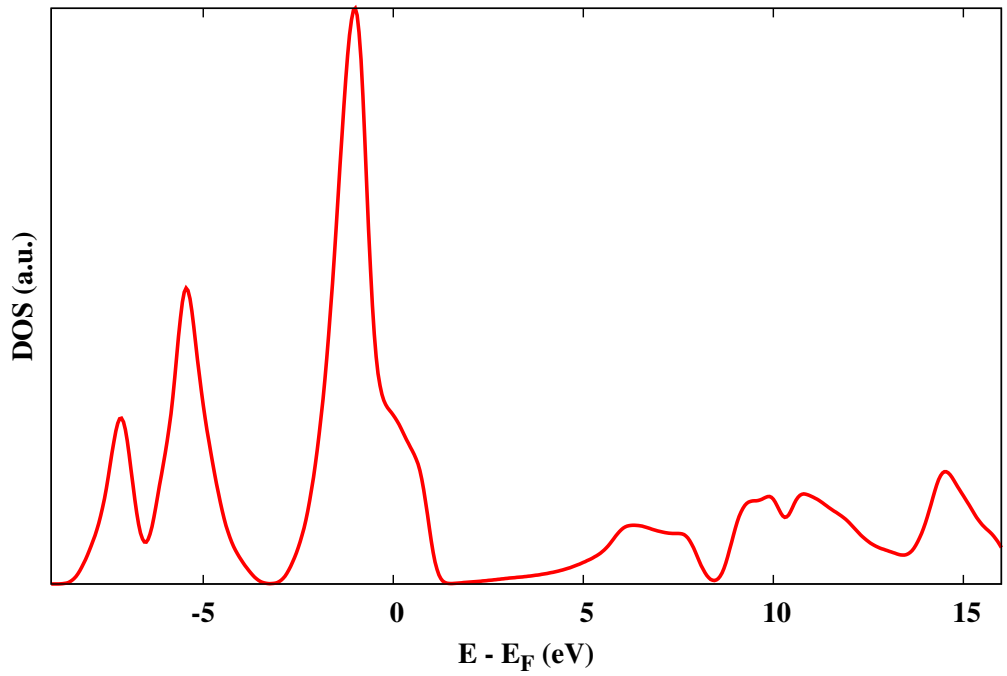

Figure 3.9: Density Of States for the Kohn-Sham system of nickel oxide obtained with an LDA calculation. The Fermi level is set at 0 eV. The non-zero DOS at E_F corresponds to a metallic behaviour. A gaussian broadening of 0.2 eV is added to the spectrum.

lation shows that considering the anti-ferromagnetic ordering gives an energy-gap, even with an improper tool like K-S LDA. It is well known that the band-gap of the Kohn-Sham system underestimates the real gap, so it is not surprising to find such a small value. Also in the anti-ferromagnetic case, one can assign the bands to contributions from the different ions. The general behaviour of the bands does not go very far from the paramagnetic case. The lower valence bands are the oxigen *p* and there is a small gap between them and the upper *d* bands, as before. The top-valence bands are *d* from nickel, but the fundamental difference with respect to the paramagnetic case is that the e_g bands are split in two parts, one in valence and the other in bottom-conduction (See Figure 3.10). This splitting is made possible by the magnetic ordering of the electrons [11, 12]. The upper conduction bands are, as in the paramagnetic case, Ni *s* and O *p* bands.

The character of the bands is an interesting aspect of the electronic structure of solids and it is referred to the electronic shells *s*, *p*, *d* and so on. Projecting the wavefunctions on the basis of spherical harmonics centered on each atom, one can evaluate how the atomic character of the electrons changes in the solid and what are the possible hybridizations, as it happens in molecules. The projected DOS concerns only one nickel atom and one oxigen of the unit cell, since the other two atoms are configured in the exact same way, but with opposite spins. The projected density of states shows very well that the top-valence and bottom-conduction bands have a Ni *d* character, while the deeper valence states have a major *p* contribution from the oxigen.

The LDA density of states is compared to the experimental data of direct (XPS) and inverse (BIS) photoemission in Figure 3.12. The most apparent thing is the highly underestimated energy-gap — 0.7 eV in LDA vs experimental 4.3 eV. Moreover, the whole of the empty states are completely off. The only structure that is fairly reproduced is the so-called *quasiparticle peak* composed by nickel's *d* bands. The gap between the oxigen *p* bands and the nickel *d* bands is not found in the experimental spectrum and it is very hard to fins a correspondence between theory and experiment for the other peaks.

The fact that the Kohn-Sham LDA band-structure in the two magnetic phases of nickel oxide give results very different from the experimental, should not worry us too much. I have compared the photoemission experimental data with the LDA DOS because this procedure has proven to give results in fair agreement with experiment for a large variety of materials. However, the Kohn-Sham LDA is an approximation born to solve the density-functional theory, a *ground-state* method. Moreover, the Kohn-Sham wavefunctions and eigenvalues do not have any physical meaning. Their only connection to the real world is the total ground-state density. They are not supposed to give any kind of description of excited-state properties. Hence, the only surprising thing is that K-S LDA gives good band structures for some materials and only others — like NiO — exploit the limits of its improper

use in describing excited states. Other methods — like *GW* — are built on purpose to describe excited states, thus we should expect better results from the application of these methods on nickel oxide.

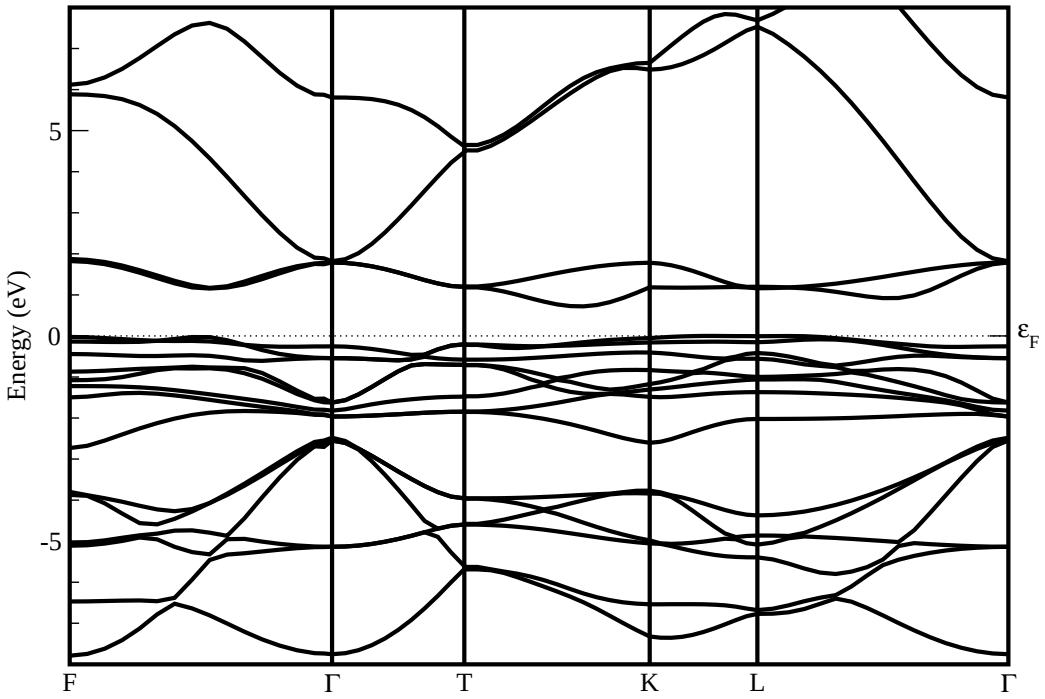

Figure 3.10: Kohn-Sham band structure of nickel oxide obtained with an LSDA calculation. The crystal structure is rhombohedral. The special points are characteristic of the rhombohedral Brillouin zone. The Fermi level ε_F is set at 0 eV. The energy gap value is 0.72 eV. Compared to the LDA band structure, here we have twice the number of bands since the unit cell is doubled and with it the number of electrons as well.

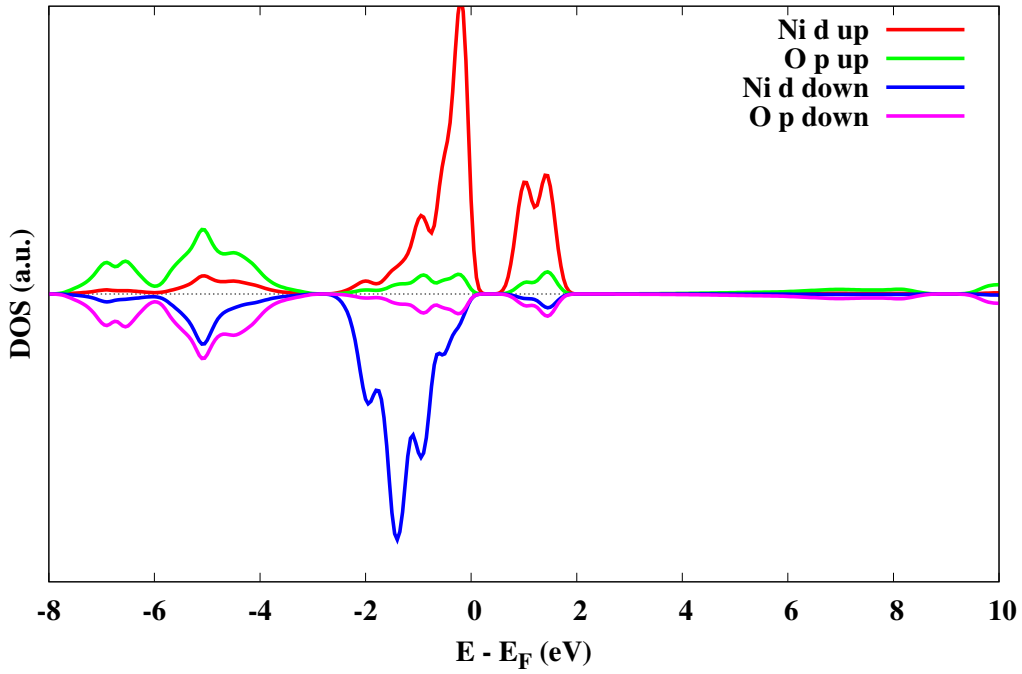

Figure 3.11: Density Of States projected on the angular components for the LSDA calculation of anti-ferromagnetic nickel oxide. One can separate (there is also a small energy-gap between them) the valence bands in two types: Ni *d* and O *p*. The top-valence is mainly Ni *d*, as the bottom-conduction. The Fermi level E_F is set at 0 eV. A gaussian broadening of 0.2 eV is added to the spectra.

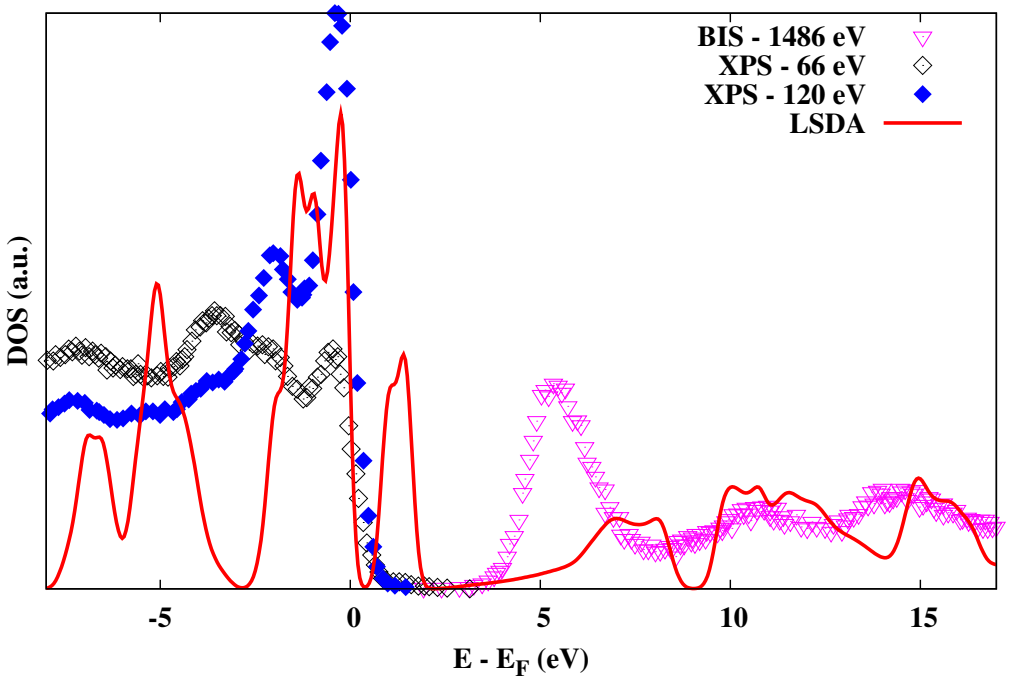

Figure 3.12: Density Of States for the Kohn-Sham system of nickel oxide obtained with an LSDA calculation. The Fermi level E_F is set at 0 eV. The calculated DOS is compared to the experimental direct (XPS) and inverse (BIS) photoemission spectrum. The calculated energy gap value is 0.7 eV. The experimental value is 4.3 eV. A gaussian broadening of 0.15 eV is added to the theoretical spectrum.

3.5 A Hartree-Fock study of NiO

The aim of this section is to point out the importance of the exchange interaction in the physics of bulk NiO. A clear description of the exchange interaction is crucial for the comprehension of the correlation effects. The calculation of the electronic structure with an exact description of the exchange between the electrons can be a reference to understand what are the effects of correlation on the system. Since correlation is defined as *everything beyond the Hartree-Fock approximation*, the electronic structure of nickel oxide has been calculated using the H-F approximation that, by construction, takes into account only exchange, i.e. only the fact that we are dealing with quantum particles, namely fermions. Particularly, we want to see if exchange plays a significant role in the paramagnetic phase, where the Kohn-Sham band structure is metallic. It is known that, for solids, the Hartree-Fock approximation highly overestimates energy-gaps. In fact, in general it is not a good method to describe bulks, while it can be a useful tool to describe isolated systems like atoms or molecules. The overestimation of the gap value in solids points out that exchange in general contributes to the opening of the gap while correlation's trend is to close it. This point of view is very clear in the framework of the *GW* approximation for the self-energy, where the Hartree-Fock approximation is recovered as a limit, when the screening ε^{-1} is put equal to 1. Hence, in *GW* all the correlation effects are included in the screening. *GW* and HF calculations give, for insulators, very different energy-gaps and the HF value is always much bigger than the *GW* one, by two or three times. The role of the screening in determining the value of the gap is then clear. In this kind of picture, too much correlation in a system should cause a metallic behaviour. This is not to be confused with the concept of *strong correlation*, often too much used and abused. In fact, strong correlation is used to describe in general many-body phenomena that are not reduceable to single-particle processes and the physics underlying these phenomena are still under heavy debate.

3.5.1 Paramagnetic phase

The electronic structure of paramagnetic NiO in Hartree-Fock is very different from the LDA one. In fact, the density of states has dramatically changed in the proximity of the Fermi level and the quasi-particle peak of the Ni *d* bands has completely collapsed (See Figure 3.13). Probably the majority of the spectral weight of the valence bands has moved to the structure at 10-15 eV below the Fermi level. Nonetheless, there is still a portion of non-zero density at 0 eV, i.e. at the Fermi level. These bands are probably the upper e_g bands, that also in the LDA case cross the Fermi level. The conduction bands appear to be shifted by about 5 eV, but do

not seem to have changed much. The system is thus predicted to be metallic by a Hartree-Fock study. The same result than in LDA.

This kind of result would lead to the conclusion that the exchange interaction is not responsible of the insulating nature of nickel oxide in the paramagnetic phase. This is somewhat reasonable, but the truth is actually far from being as clear as that. This issue will be better developed in the following chapters and the analysis of the other calculations performed and of the result in literature will help to obtain a more complete picture of the problem.

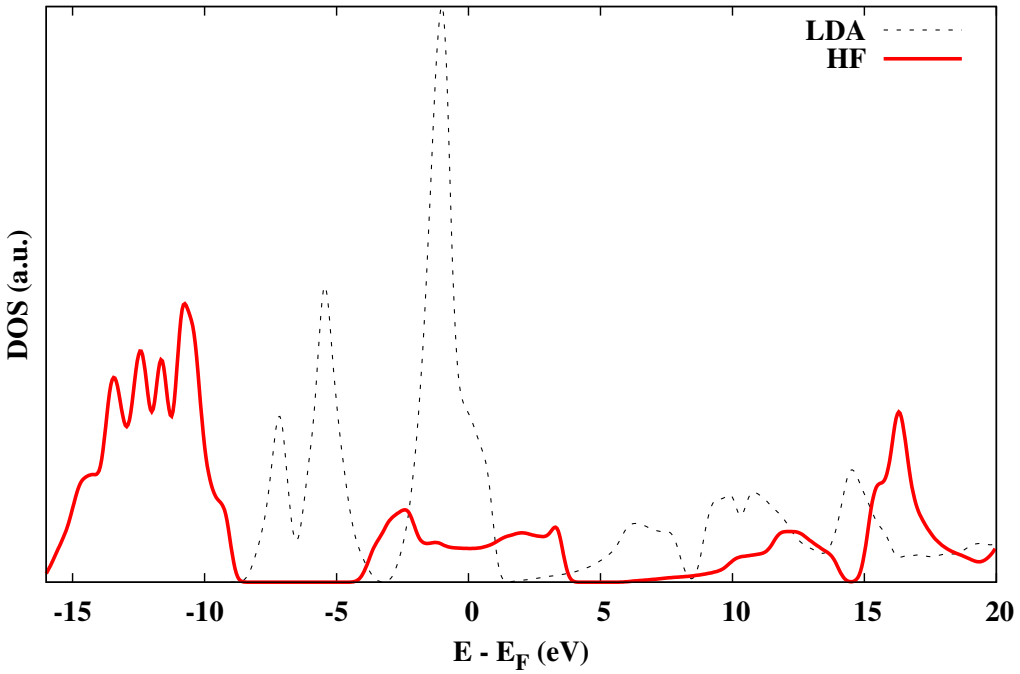

Figure 3.13: Density Of States for the Hartree-Fock calculation of nickel oxide. The Kohn-Sham LDA DOS is shown for comparison. The Fermi level E_F is set at 0 eV. The predicted behaviour is still metallic as the DOS is non-zero at the Fermi level. A gaussian broadening of 0.2 eV is added to the spectrum.

3.5.2 Anti-ferromagnetic phase

The Hartree-Fock density of states has dramatically changed also compared to the LSDA. The gap is present indeed, but its magnitude is of about 14 eV. The LSDA energy-gap was 0.7 eV. The quasiparticle peak has moved far from the Fermi level, leaving a huge gap. The experimental photoemission gap is reported to be 4.3 eV.

The Hartree-Fock calculation is too far from any reasonable comparison with experiment. As already remarked, this is a known behaviour of Hartree-Fock calculations on solids. The correct treatment of exchange causes a strong localization of the wavefunctions, that leads to a highly overestimated energy-gap. In this picture, the role of correlation would be to reduce the exchange effects, i.e. to reduce the value of the band-gap. In fact — as explained in the theoretical introduction — a study of nickel oxide with methods derived from the Green's function theory is expected to give a better description of the system, since both exchange and correlation are taken into account properly.

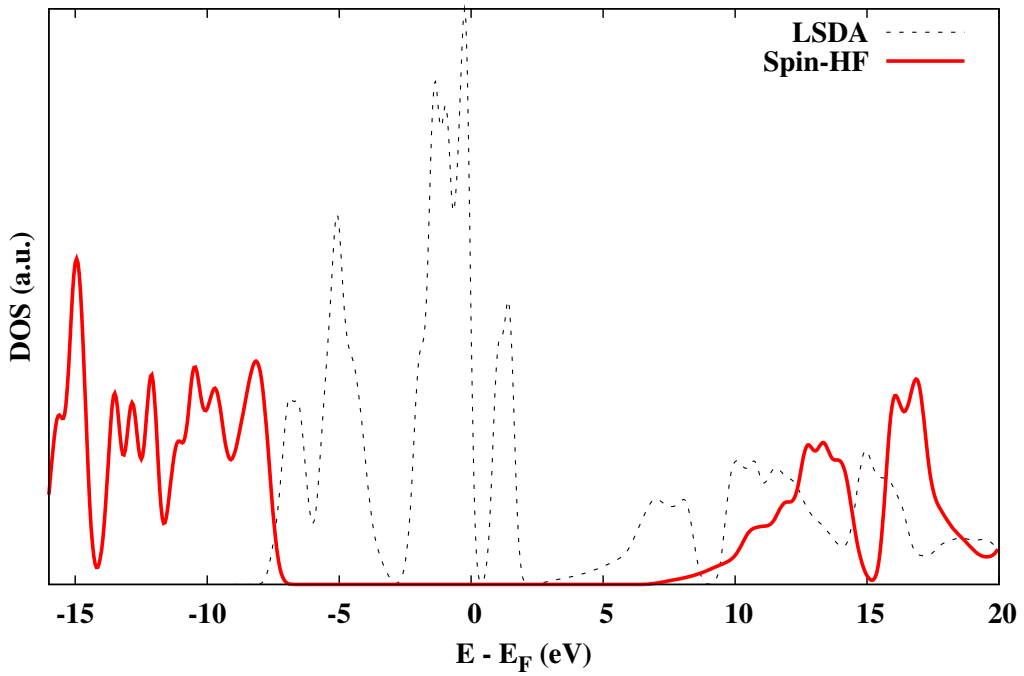

Figure 3.14: Density Of States for the spin-polarized Hartree-Fock calculation of nickel oxide. The Kohn-Sham LSDA DOS is shown for comparison. The Fermi level E_F is set at 0 eV. The energy-gap is of about 15 eV. This largely overestimated gap value is a common feature of Hartree-Fock calculations on solids. A gaussian broadening of 0.2 eV is added to the spectrum.

Chapter 4

A *GW*-and-beyond study of NiO

This chapter discusses the analysis of NiO by means of the *GW* method with different approximations, perturbatively or self-consistently. The analysis will concern the anti-ferromagnetic phase, as pointed out before. My concern will be now on the photoemission spectrum of nickel oxide and on the magnitude and origin of the energy-gap. To fulfil this task we will make use of some of the most advanced tools available admist the *ab-initio* theoretical tools. These are the *GW* method, derived from Many-Body Perturbation Theory, and other approximations for the self-energy, such as the COHSEX and the *GW*Γ.

4.1 Perturbative *GW*

I have applied the standard *GW* approach on nickel oxide. This method is built to describe properly the quasiparticle excitation energies, i.e. the addition and removal energies in a photoemission experiment. The *GW* energies are calculated as first-order corrections of the LDA eigenvalues. The density of states of the *GW* calculation is shown in Figure 4.1. It is compared with the experimental data. The calculated photoemission gap value is 1.7 eV. It is much smaller than the experimental one (4.3 eV). There is an appreciable change in the valence bands: the width in energy of the occupied states goes from 8 eV to about 6.3 eV. The main *d* peak is now wider and the gap between O *p* and Ni *d* in valence has closed. The second *d* peak seems to have too much spectral weight and to have a wrong energy, if it is compared with the second structure in the 120 eV XPS spectrum. The third structure, well visible in the 66 eV XPS spectrum, appears correctly reproduced, even though a lot of spectral weight between *p* and *d* peaks is missing. The conduction bands, apart from a rigid shift of 2-3 eV, look in fair agreement with the BIS data if one compares the reciprocal positions of the peaks. There is an overall bad agreement of the calculation with the experimental spectrum, nevertheless

the *GW* corrections go in the right direction regarding the energy-gap. There is an improvement with respect to LDA. The valence bands, instead, show only little change with respect to LDA, and it is not clear wether it is better or worse.

We known from literature that a perturbative *GW* calculation applied on transition-metal oxides is not able to give a correct description of the photoemission spectrum. This is reported to be mainly an effect of the poor LDA starting point. Nevertheless I included this part in the thesis, to show how standard *GW* performs on NiO. In the next section, I will carry out a more detailed discussion on the reasons of the failure of the standard *GW* approach on nickel oxide.

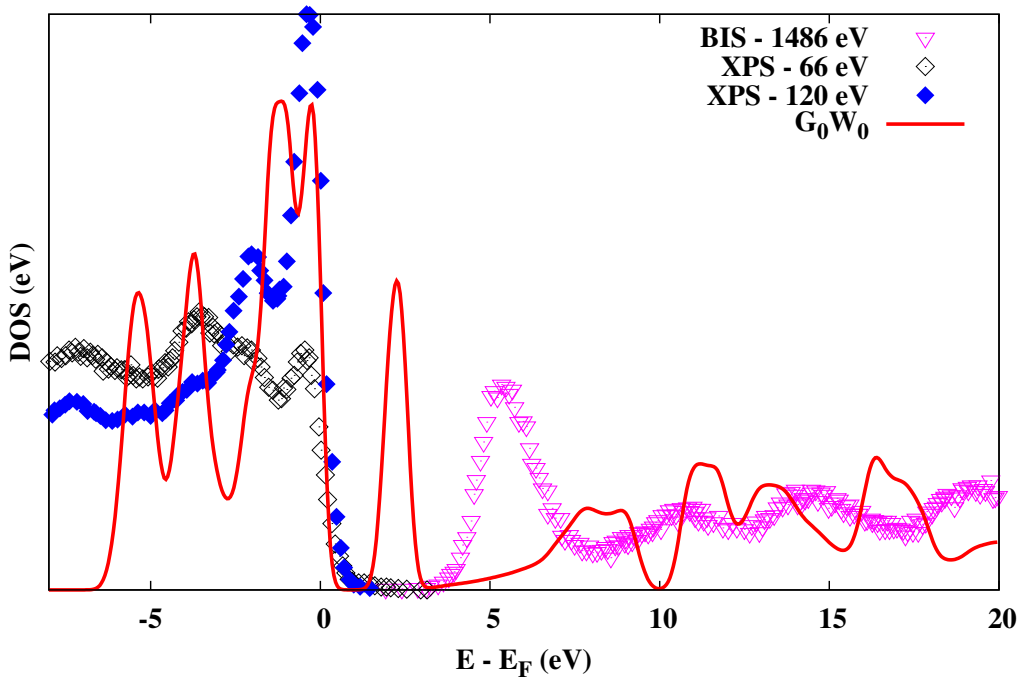

Figure 4.1: Density of states (DOS) for the perturbative *GW* calculation of nickel oxide. The experimental direct (XPS) and inverse (BIS) photoemission data are shown for comparison. The experimental photoemission gap is 4.3 eV. The *GW* energy-gap is about 1.7 eV. The calculation is in bad agreement with the experiment, nevertheless the energy-gap is much wider that in the LDA case and the DOS shows better agreement in valence and conduction. The Fermi level E_F is set at 0 eV. A gaussian broadening of 0.2 eV is added to the spectrum.

4.2 Self-consistency and alternative approaches

The failure of the perturbative *GW* method on NiO is somewhat expected, in fact the literature about transition metal oxides described by means of *ab-initio* methods is quite assertive in this sense. One reason often reported to cause bad results is a too strong delocalization of the LDA wavefunctions. In fact, the LDA exchange-correlation potential in Kohn-Sham system cannot give a good description of the exchange interaction between *d* electrons, that are very localized in space, as reported by Aryasetiawan *et al.* [18]. Also, the LDA ingredients used to calculate the screening in Σ, in the standard *GW* perturbative approach, appear to affect too much the *GW* corrections [20]. In fact, the screening generated from a Kohn-Sham system with such a small band-gap is too strong and leads to small gaps. In general, a strong screening leads to semiconductors or metals — whereas Hartree-Fock, where the screening is neglected, leads to high gap insulators. In a one-step procedure, it is crucial that all the ingredients are not too far from the final point. Taking a starting point with a wider gap has been reported to improve the *GW*-on-LDA result [21], giving a wider final gap. A better starting point — i.e. in most cases a wider gap — can be achieved either using an exchange-correlation functional different from LDA, like GGA or hybrids, or applying a scissor operator to the Kohn-Sham eigenvalues. Another solution would be to continue and iterate the *GW* approach, updating the quasiparticle energies at each step and stopping when the energies have reached self-consistency. Li, Rignanese and Louie have applied one of this approaches to nickel oxide using a GGA exchange-correlation functional [21] and a plasmon-pole model W. This is a quite affordable approach, since it costs only $\sim N$ times the computational cost of a *GW* calculation, where N is the number of iterations[1]. The band-gap obtained by such method is $E_g = 2.9$ eV, which is better than the *GW*+LDA and goes in the right direction, but still not in good agreement with the experimental data. The approach of Aryasetiawan and Gunnarsson [18] is quite similar, as they carry out a *GW* calculation self-consistent for the energies within the LDA. However, they do not adopt the plasmon-pole model for W. They use a *Linear Muffin-Tin Orbitals* basis (LMTO) for the wavefunctions. Moreover, they add a non-local potential of ~ 6 eV to the e_g bands of the nickel, to simulate the effects due to the change of the wavefunctions. The calculated band-gap is $E_g \sim 5.5$ eV, still quite different from the experimental one (4.3 eV). The possibility of using hybrid functional has been explored, but issues remain on the reliability of this method, since several arbitrary parameters enter in the calculation and the physical meaning of the Kohn-Sham orbitals remains theoretically doubtful. Massidda *et al.* [19], instead, adopt a fully self-consistent approach in energies and wavefunctions, but they use a model self-energy to make

[1] Supposing that the number of iterations N is on the order of 10.

computation feasible. The energy gap they find is $E_g = 3.7eV$. Among the examples that have been described here it is the value of the energy-gap closest to experiment, but having a model Σ makes it difficult to compare this result with others and to evaluate the actual validity of the method.

All the approaches described above try to go beyond the perturbative approach in *GW* and point out the need of a self-consistent calculation, to get appropriate wavefunctions. They point out that in the case of transition-metal oxides it becomes necessary to get rid of a too poor starting point, i.e. the Kohn-Sham wavefunctions. However, they never apply a full self-consistent approach, basically because it would be too heavy computationally. So they find a compromise to get to a result in a feasible way. Thus, different compromises (and different approximations) bring different results, as one can see from the fair range of energy-gaps found. This way, the physics of the photoemission process in NiO remains without a satisfactory explanation.

To get a reliable result, one needs to get rid of the dependence from a poor starting point like LDA or GGA and find a proper description for the wavefunctions. The straight-forward solution would be to perform a full self-consistent *GW* calculation, solving self-consistently the quasiparticle equation of motion. This is a quite heavy calculation, since one needs to diagonalize a complex, non-local and energy dependent operator. Moreover, since Σ^{GW} is not hermitian, one has to find a hermitian approximation as well. Faleev *et al.* [20] carried out this approach. In their publication they include the full energy dependence of W without plasmon-pole model, but neglect the so-called *incoherent* part of the self-energy, which gives rise to satellites. They call this procedure *QuasiParticle self-consistent GW* (QPscGW). Not using the plasmon-pole model, while keeping more reliability, raises even more the computational effort needed for the calculation. Moreover, they treat explicitly all the electrons of the system (the so-called *all-electron* treatment) adding weight compared with my pseudopotentials calculations. Nevertheless, their approach brings to a good agreement with the experimental photoemission data. The calculated photoemission gap is $E_g = 4.8$ eV.

One would like to have a cheaper approach that could give us similar results. A possibility is to use the COHSEX approximation for the self-energy. The Σ^{COHSEX} is hermitian, static and depends only on the occupied states of the system. Consequently, it is much cheaper to calculate with respect to the full Σ^{GW}. To include the dynamical effects of the latter, one performs a one-shot *GW* calculation on top of the converged COHSEX quasiparticle band structure. The main pourpose of the self-consistent approach is to modify the wavefunctions. The COHSEX approximation has shown to be appropriate for this task on different transition-metal oxides like Cu_2O [34] and VO_2 [35]. Performing a full *GW* perturbative step on the COHSEX band structure properly includes the dynamical effects in the calculation. With this approach it is possible to get results quite similar to a fully self-consistent

GW approach, but with at least an order of magnitude less in terms of calculation time [34].

Moreover, the self-consistent COHSEX approach permits one to get rid of the starting point dependence that introduced a sort of arbitraryness in the *GW* method, namely to not depend on the Kohn-Sham wavefunctions anymore.

4.2.1 Self-consistent COHSEX in practice

To make the self-consistent approach feasible, the quasiparticle COHSEX wavefunctions are expanded in the basis set of LDA Kohn-Sham orbitals as follows:

$$|\phi_{i\mathbf{k}}^{\mathrm{QP}}\rangle = \sum_j c_{ij\mathbf{k}}.|\varphi_{j\mathbf{k}}^{\mathrm{LDA}}\rangle \tag{4.1}$$

The projection coefficient are defined as $c_{ij\mathbf{k}} = \langle\varphi_{j\mathbf{k}}^{\mathrm{LDA}}|\phi_{i\mathbf{k}}^{\mathrm{QP}}\rangle$. The quasiparticle wavefunctions are thus constrained to be linear combinations of LDA wavefunctions. The reliability of this procedure has been discussed by F. Bruneval *et al.* [34, 36] and M. Gatti [35] in previous works on transition-metal oxides.

Our aim is to solve the quasiparticle equation (2.26) in the COHSEX approximation. At each step, using the quasiparticle wavefunctions $\varphi_{i\mathbf{k}}$ and the quasiparticle energies E_i, one has to calculate the full Hamiltonian $\langle\phi_{i\mathbf{k}}|h_0 + \Sigma|\phi_{j\mathbf{k}}\rangle$, where Σ is the static and Hermitian COHSEX self-energy. In particular one needs to calculate ε^{-1} and W at $\omega = 0$ to build Σ before each step. At the step n, the diagonalization of the Hamiltonian yields a new set of quasiparticle energies $E_i^{(n)}$ and coeffcients $c_{ij\mathbf{k}}^{(n)}$ that link the new quasiparticle wavefunctions to the quasiparticle wavefunctions at the previous iteration:

$$|\phi_{i\mathbf{k}}^{(n)}\rangle = \sum_j c_{ij\mathbf{k}}^{(n)}|\phi_{j\mathbf{k}}^{(n-1)}\rangle. \tag{4.2}$$

So the matrix of the coeffcients evolves through the self-consistent loop, by mixing for each quasiparticle wavefunction $\phi_{i\mathbf{k}}$ different contributions coming from the different LDA wavefunctions $\varphi_{i\mathbf{k}}$. Since the Hamiltonian is Hermitian, the matrix of the coeffcients c_{ij} remains unitary. By converging the calculation, the Hamiltonian on the basis of the updated quasiparticle wavefunctions $\phi_{i\mathbf{k}}^{(n)}$ tends to be diagonal. One iterates the self-consistent loop until the new quasiparticle energies E(n) i are close (within a fixed small difference, in general 1 meV) to quasiparticle energies at the previous step $E_i^{(n-1)}$. Finally, the converged self-consistent COHSEX eigenfunctions and eigenvalues are used as an input for the last perturbative GW calculation that yields the final result.

The application of the self-consistent COHSEX approximation to the nickel oxide has produced an appreciable change in the band structure and in the density of states (Figure 4.2). The most apparent change is of course the energy-gap,

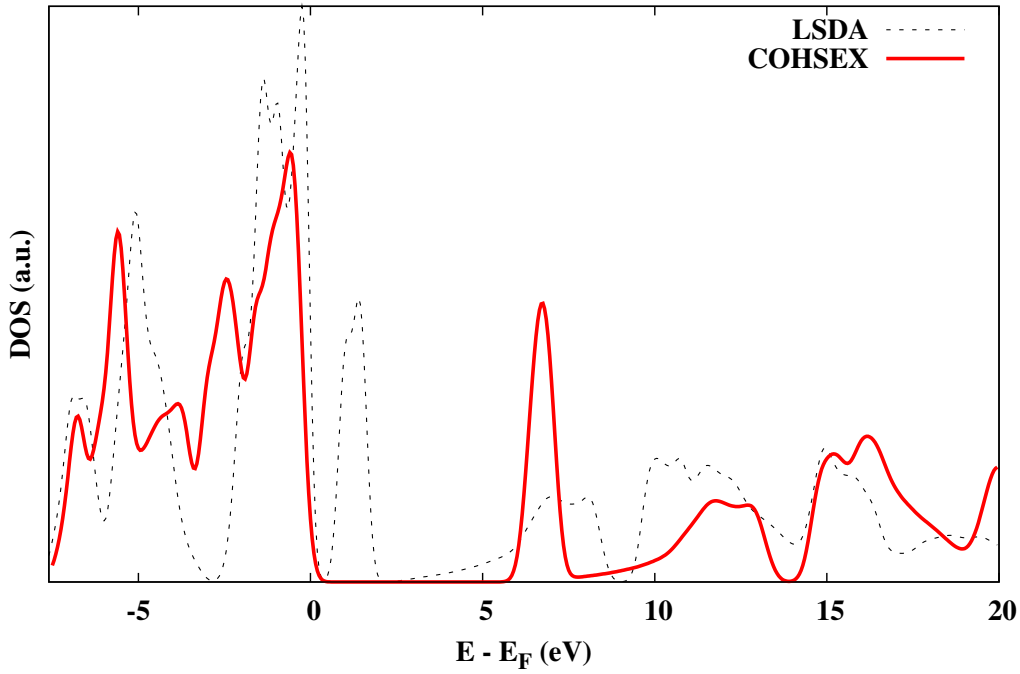

Figure 4.2: Density Of States of a self-consistent COHSEX calculation of nickel oxide in the anti-ferromagnetic phase. The energy gap is E_g=6.1 eV. The Fermi level E_F is set at 0 eV. A gaussian broadening of 0.2 eV is added to the spectrum.

that measures about 6 eV. The valence states have a quite different shape from the LDA ones while the conduction states appears to have been just shifted with respect to LDA. The shift, though, is much greater for the empty *d* states. The cause of this is the correct treatment of exchange in the self-energy, which causes an energy separation of more localized states such as the nickel *d*. At top-valence, the quasiparticle peak has appreciably decreased. The small energy-gap in the middle of valence bands has disappeared.

4.2.2 Hybridization in COHSEX band structure: projected density of states

I compared the projected DOSes of LDA and self-consistent COHSEX to see how a correct description of exchange and correlation as the one of MBPT determines hybridization and atomic character. As the COHSEX gives a quite different energy-gap and DOS with respect to LDA, we expect to see some differences.

In Figure 3.11 the projection of the Kohn-Sham DOS on two different angular components is displayed, i.e. the oxygen *p* and the nickel *d*. This bands are mainly contributing to the valence and bottom-conduction bands, which are the bands we are most interested in. The valence bands are filled by O *p* and Ni *d* type electrons, while the conduction bands are mainly Ni *d* near the gap and O *p* and Ni *s* (not displayed) above. In the valence bands there is an energy-gap of about 0.8 eV between O *p* and Ni *d* electrons and the top valence has an almost pure Ni *d* character. The picture also shows well how spin-polarization affects only the *d* electrons while the *p* have the same density up and down. The self-consistent COHSEX calculation yields a quite different result from LDA. In the projected DOS (Figure 4.3) Ni *p* and O *d* are displayed. As in the LDA case, only two ions out of four are reported. Apart from the wider gap, the most apparent features are a considerable hybridization of the valence bands and a higher Ni *d* contribution in the bottom-conduction bands. The valence bands now have a mixed *p*-*d* character overall. The top-valence band has much more O *p* contribution and there is a generalized Ni *d* contribution in the whole valence. There is no clear possible distinction between *p* and *d* bands. This kind of result already gives some hints about the opportunity of adopting the COHSEX approximation. The hybridization of the valence bands shows that the LDA electronic structure is actually a poor description of NiO, not reliable at all. The dramatic change in the valence bands suggests that the LDA wavefunctions are not adequate as a starting point of a *GW* calculation. A more accurate analysis of the wavefunctions, though, requires to take into account the variations of single wavefunctions.

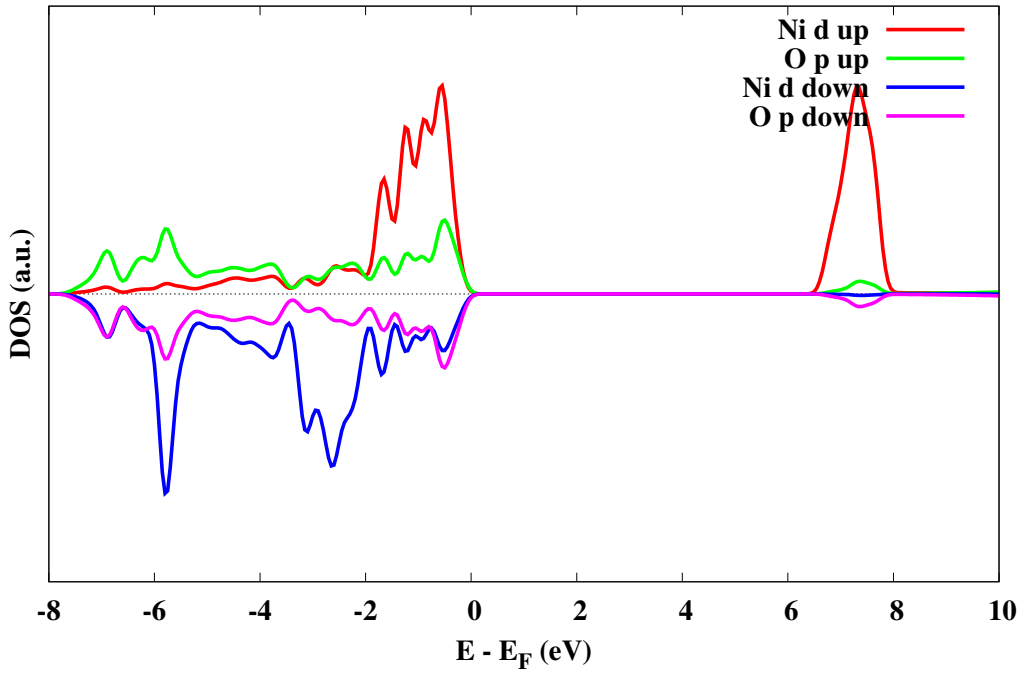

Figure 4.3: Density Of States projected on the angular components for the self-consistent COHSEX calculation of anti-ferromagnetic nickel oxide. The valence bands cannot be clearly distinguished between Ni *d* and O *p*, namely, the top-valence has a marked contribution from O *p*, while it loses some Ni *d* weight. The bottom-conduction bands is of Ni *d* type and it gains more weight compared to LDA. The Fermi level E_F is set at 0 eV. A gaussian broadening of 0.2 eV is added to the spectra.

4.3 A look onto the wavefunctions: LDA vs COHSEX

The angular-momentum projected DOS shows a dramatic change at the level of valence electron, where there is a strong mixing of bands, whereas the Kohn-Sham valence orbitals were quite well separated in oxygen *p*s and nickel *d*s. But the projected DOS does not tell anything about the modification of single wavefunctions. That is why it is necessary to evaluate directly how the single wavefunctions change. This can be done evaluating the projection of the wavefunctions on the basis.

To evaluate the differences between COHSEX and LDA wavefunctions I took, for each COHSEX band and k point, the maximum value of the projection coefficient on the LDA wavefunctions. In other words, this number evaluates the least change of the wavefunction in a defined k point. Formally, it is defined as

$$\max_j |c_{ij\mathbf{k}}|^2 = \max_j \left| \langle \varphi^{\mathrm{LDA}}_{j\mathbf{k}} | \phi^{\mathrm{QP}}_{i\mathbf{k}} \rangle \right|^2 . \tag{4.3}$$

These coefficients are displayed in Figure 4.4, for bands 11–60, that have been included in the self-consistent calculation. A value of 1 for the projection means that the COHSEX wavefunction is identical to the LDA one. It appears how the quasiparticle valence bands have undergone a drastic change. The conduction bands, instead, are quite similar to the LDA ones, except for bands 25 and 26, that form the bottom conduction and have a strong Ni *d* character. Far from the gap, quasiparticle wavefunctions are not very different from LDA.

A deeper analysis can be carried out evaluating for each band the density $\rho = |\phi|$ and its variation $|\rho^{\mathrm{COHSEX}} - \rho^{\mathrm{LDA}}|$. For each band, the density is summed over all the k points in the brillouin zone. I have taken a few bands as qualitative examples. In Figure 4.5 the variation of the density of band #14 is displayed. In LDA, it has a pronounced oxygen *p* character, while in COHSEX the trend is opposite. The density decreases around the oxygen and increases around the nickel, as it can also be seen from the angular-momentum projected densities of states, Figures 3.11 and 4.3. It is interesting to see what happens in proximity of the energy-gap. The analysis of the wavefunctions helps to understand what already suggested by the projected DOS. The top-valence band, i.e. band number 24, displays in LDA a strong *d* character, as shown in Figure 4.6, localized mainly on one Ni ion. The COHSEX wavefunction, on the contrary, is quite delocalized on all the Ni and O ions. The bottom-conduction band (number 25) has a sort of opposite variation. In LDA it is mainly localized around one Ni ion, but there are moderate contributions also on the oxigen ions and (a little) on the other Ni. In COHSEX, this band is almost completely localized on one Ni ion. This opposite behaviour of these two bands suggests that there could be some reciprocal mixing, as the conduction bands

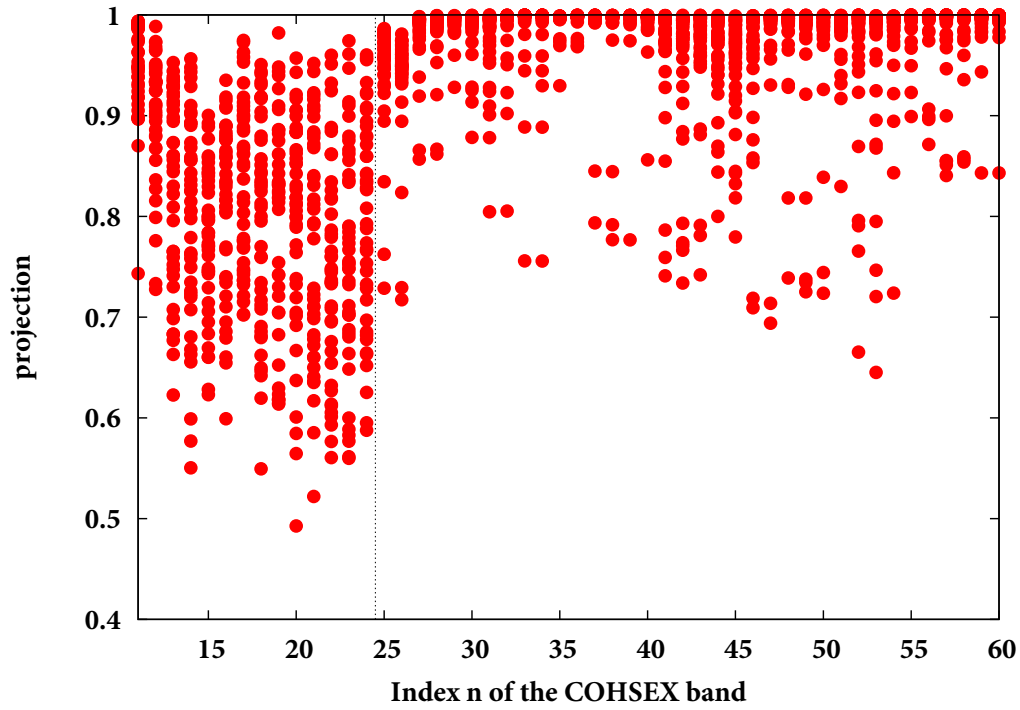

Figure 4.4: For each COHSEX wavefunction $\phi_{n\mathbf{k}}^{\mathrm{COHSEX}}$, a red dot indicates the maximum value of the projection of COHSEX wavefunction over all the LDA states $\varphi_{m\mathbf{k}}^{\mathrm{LDA}}$ of the basis (see Eq. (6.2)). At each index n the different dots correspond to the different 42 k points that have been considered. The vertical dashed line between 24 and 25 separates occupied from empty states. A value of 1 for the projection means that the COHSEX wavefunction is identical to the LDA one. The valence wavefunctions have no projections equal to one, showing a dramatic change of the COHSEX wavefunctions with respect to the LDA, while in conduction the wavefunctions are closer to LDA going further from the gap.

gain *d* weight while the top-valence loses it. Figure 4.8 displays clearly this specular behaviour of the two bands.

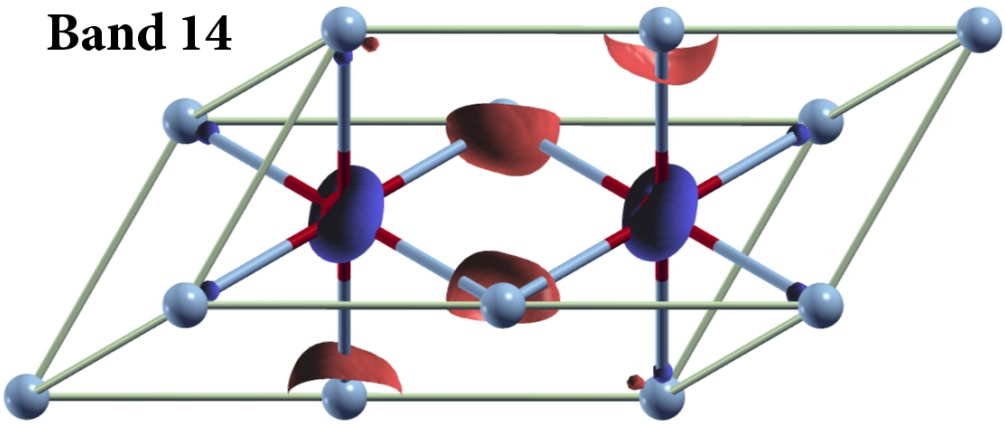

Figure 4.5: Isosurfaces of differences $|\rho^{\mathrm{COHSEX}} - \rho^{\mathrm{LDA}}|$=0.01 a.u.$^{-3}$ between LDA and COHSEX wavefunctions for band #14 in real space. Brown color is for positive variations; violet is for negative variations. Band 14 is at about 6 eV below E_F. In LDA it has mainly an O *p* character, while in COHSEX it has a greater Ni *d* component, as it is shown by the varation of the density. Please note that the isosurfaces respect the periodicity of the trigonal lattice.

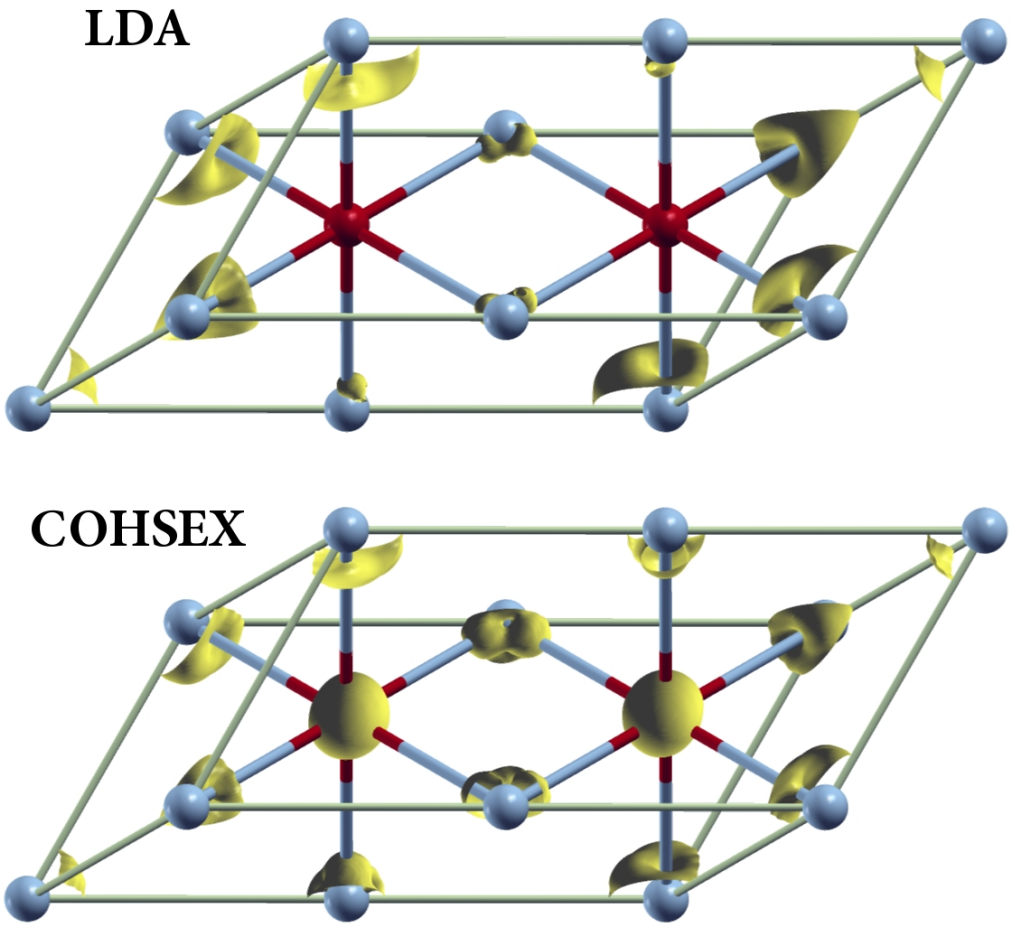

Figure 4.6: Isosurfaces of LDA (upper panel, yellow) and COHSEX (lower panel, yellow) densities of top-valence band (#24) in real space. The densities are displayed in the antiferromagnetic trigonal unit cell. The isosurfaces are traced at the value ρ=0.05 a.u.$^{-3}$. It appears how the LDA electronic density is more localized on one Ni ion (light blue), i.e. it has high *d* character and strong spin polarization. In the COHSEX case, the band gains weight on the other Ni ion and on the oxygen ions (red), being more hybridized than LDA. Please note that in this picture the isosurfaces respect the periodicity of the trigonal lattice.

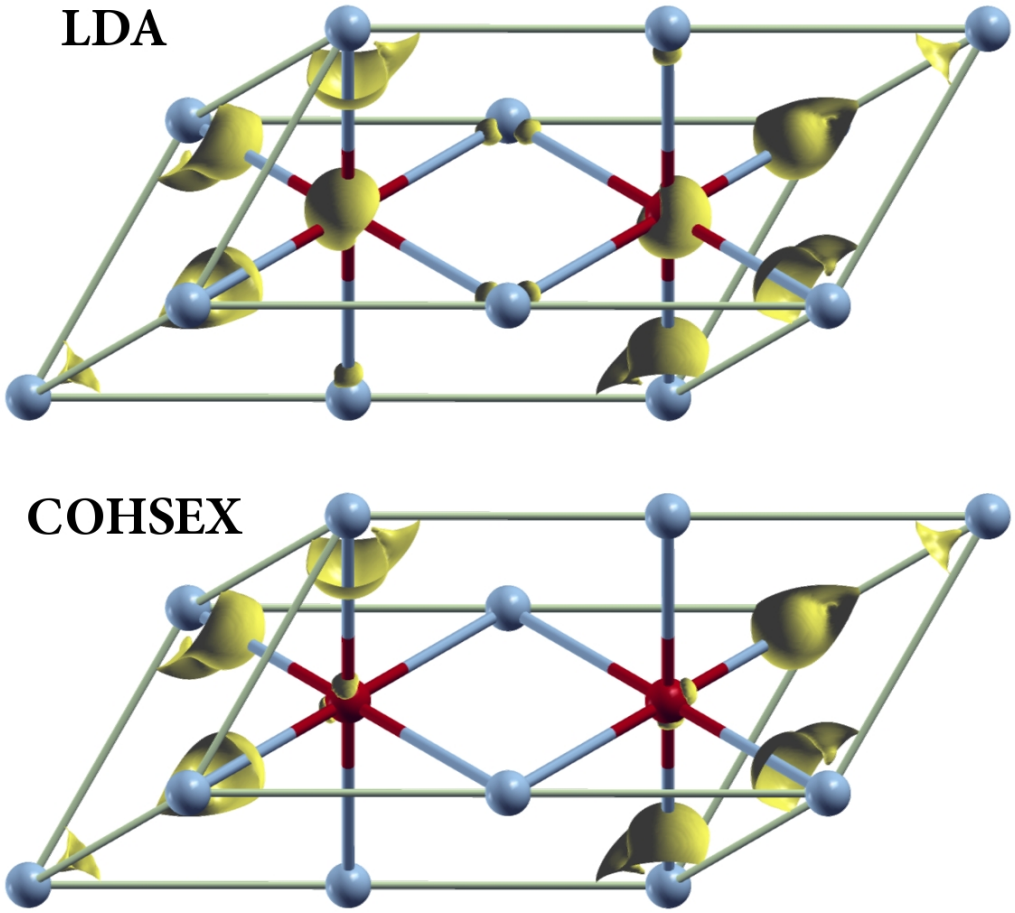

Figure 4.7: Isosurfaces of LDA (upper panel, yellow) and COHSEX (lower panel, yellow) densities of bottom-conduction band (#25) in real space. The densities are displayed in the antiferromagnetic trigonal unit cell. The isosurfaces are traced at the value ρ=0.03 a.u.$^{-3}$. It appears how the LDA electronic density has a major contribution from one Ni ion (light blue) and a minor contribution from the other Ni and the oxigen ions (red). In the COHSEX case, the band gets less hybridized, i.e. the contribution to the density comes mainly from one *d* ion, as one can see also from the angular-momentum projected DOS in Figure 4.3. Please note that in this picture the isosurfaces respect the periodicity of the trigonal lattice.

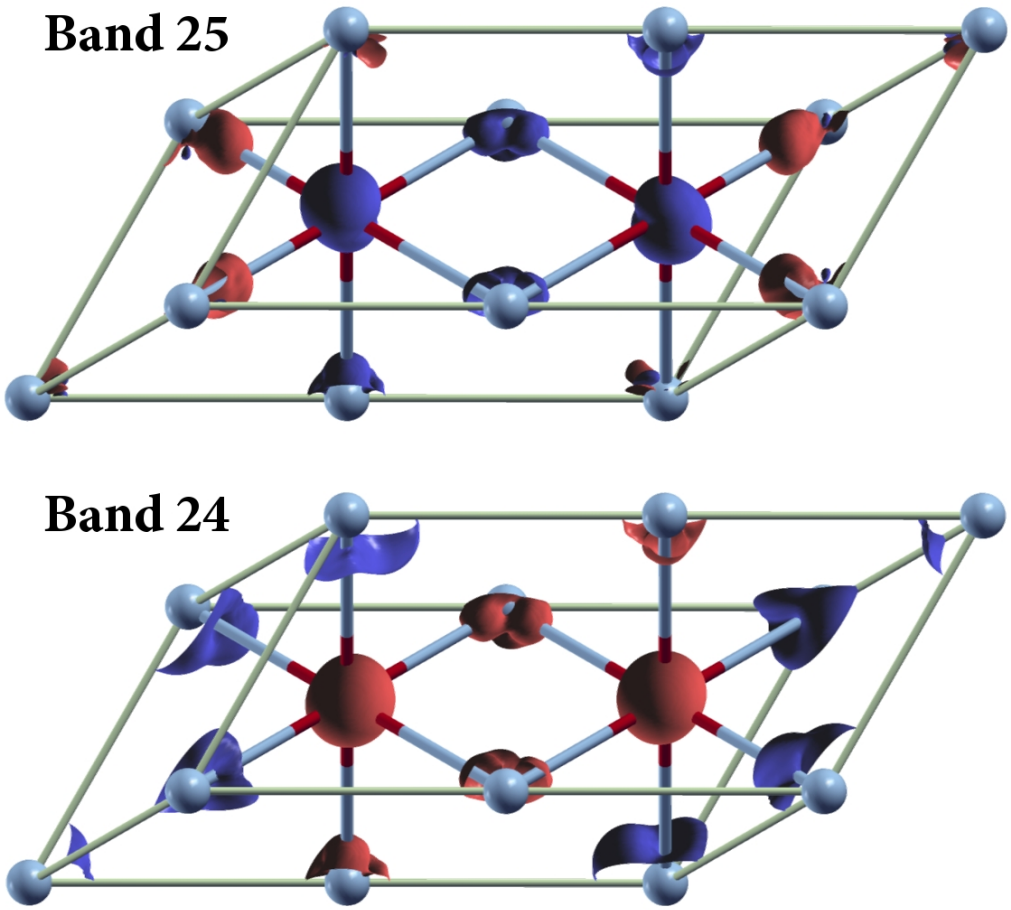

Figure 4.8: Isosurfaces of differences $|\rho^{\mathrm{COHSEX}} - \rho^{\mathrm{LDA}}|$ between LDA and COHSEX wavefunctions for bottom-conduction (upper panel) and top-valence (lower panel) bands (25 & 24) in real space. Brown color is for positive variations; violet is for negative variations. For band 25 $|\rho^{\mathrm{COHSEX}} - \rho^{\mathrm{LDA}}|$=0.01 a.u.$^{-3}$. For band 24 $|\rho^{\mathrm{COHSEX}} - \rho^{\mathrm{LDA}}|$=0.03 a.u.$^{-3}$. The picture shows how the two bands have opposite trends. Top-valence gets more hybridized while bottom-conduction gets more *d* atomic character. Nickel ions are in light blue. Oxygen ions are in red. Please note that the isosurfaces respect the periodicity of the trigonal lattice.

4.4 *GW* on top of COHSEX

Once we have calculated the COHSEX wavefunctions and energies, we have a reliable starting point from which we can calculate the *GW corrections*. The *GW* energies are calculated as a first-order perturbation of the COHSEX quasiparticle energies. The *GW* self-energy includes all the dynamical effects that were neglected in the COHSEX approximation, thus being in principle very close to the QPscGW approach. The calculated photoemission spectrum is displayed in Figure 4.9 and compared with the experimental data from Sawatzky *et al.* [7]. The spectrum shows overall good agreement with experimental data. The calculated energy gap is about 5.4 eV. However, the fact that we have a discrete mesh in the reciprocal space can affect this value if we miss some important k points. Namely, I am carrying out some calculations on different grids that reveals how the bottom-conduction minimum should be located in the Γ point. This point is not included in the present grid and I estimate the actual GWonCOHSEX gap to be about 0.5 eV smaller than the present result, thus giving about 4.9 eV of energy band-gap. This result is not so close to the experimental value, although closer than the majority of other *GW* approaches. Moreover, it is very close to the value obtained by Faleev *et al.* [20], thus exploiting the validity of GWonCOHSEX as an affordable and reliable self-consistent method.

The valence bands are well reproduced. All the peaks from 0 to 7 eV below the Fermi level are reproduced in the calculation. The -8 eV satellite is not reproduced. The analysis of the satellites would require an explicit calculation of the spectral function, but this goes beyond the scope of this thesis. Moreover, self-consistency has been reported to cause an underestimation of satellite structures in photoemission [46]. The upper conduction bands show also a fair agreement with experimental data: all the peaks above the bottom-conduction are rigidly shifted by about 1 eV, yet, they are correctly reproduced. However, using the plasmon-pole model for our calculations lowers its reliability for the upper conduction bands [34]. The photoemission spectrum calculated by means of the GWonCOHSEX approach gave a satisfactory result. Combining self-consistency with the standard perturbative *GW* method has given similar result to QPscGW, a self-consistent approach that has a greater computational drawback with respect to my approach.

At this point, it can be interesting to see if this results can be improved using an approximation better than *GW*. The next section will clarify this issue.

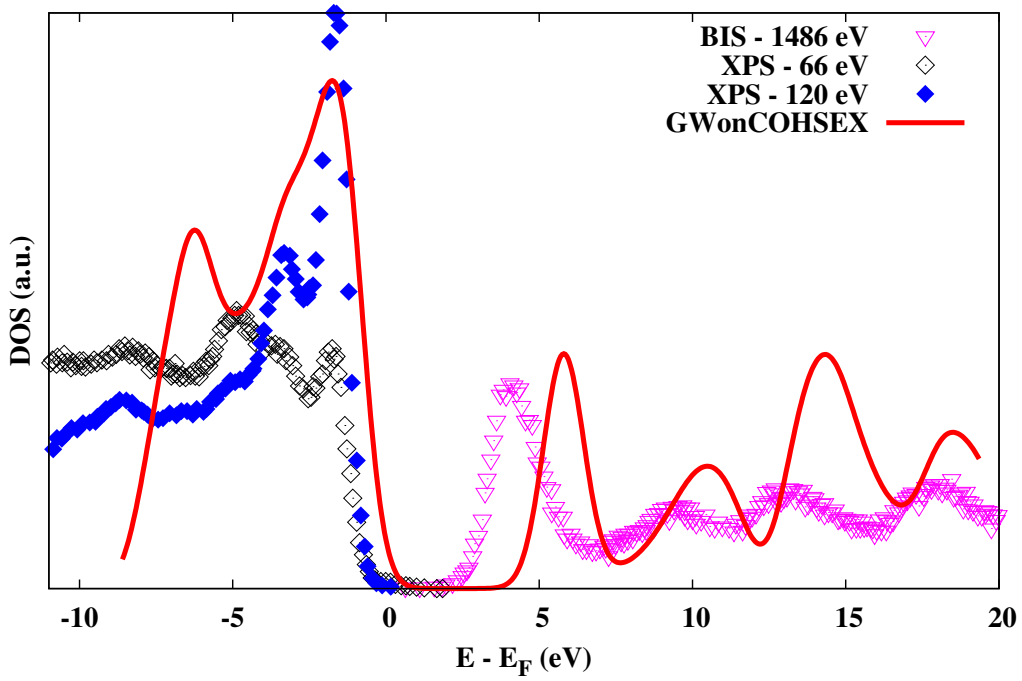

Figure 4.9: Density Of States of a perturbative *GW* calculation on top the converged COHSEX band structure of nickel oxide in the anti-ferromagnetic phase. The theoretical spectrum is compared to the experimental XPS and BIS data. The experimental energy-gap is about 4.3 eV. The calculated energy gap, considered the missing k points, is E_g=4.9 eV. The Fermi level E_F is set at 0 eV. A gaussian broadening of 0.6 eV, equal to the uncertainty of the data, is added to the spectrum.

4.5 Vertex corrections to the self-energy

The GW approximation is an approximation for the self-energy derived through Hedin's equations. Actually, in its exact form, the self-energy is written as $\Sigma = iGW\Gamma$, where Γ is the so-called *vertex function*. I have performed a perturbative calculation within the $GW\Gamma$ approximation, i.e. including vertex corrections, as reported in References [37]. The procedure is exactly the same as GWonCOHSEX, but the last step is done within the $GW\Gamma$ approximation.

The comparison between GWonCOHSEX calculation and the $GW\Gamma$ one shows how the inclusion of vertex corrections in the self-energy does not change the spectrum in an appreciable manner. There is a slight change in the valence bands, but it is very small. The two curves are compared in Figure 4.10 and they are well within the error of the approach, which is around 0.1 eV. Thus, the vertex corrections do not appear to have an important role in the photoemission spectrum of nickel oxide. Nevertheless, the approximation adopted for the vertex is very simple in order to be tractable. Better approximations might exploit effects that here are neglected.

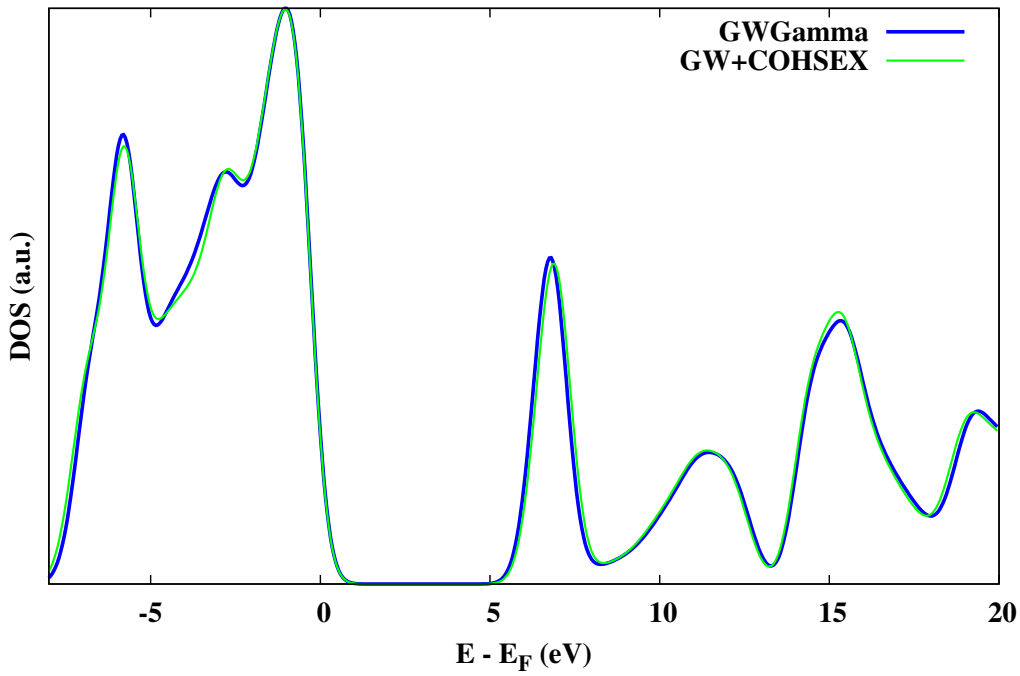

Figure 4.10: Density Of States of a perturbative $GW\Gamma$ (i.e. including vertex corrections) calculation on top of the COHSEX band structure of nickel oxide in the antiferromagnetic phase. The spectrum is compared with a perturbative *GW* calculation. They are almost identical. The Fermi level E_F is set at 0 eV. A gaussian broadening of 0.2 eV is added to the spectrum.

Chapter 5

Conclusion

— …Attention à la marche
en descendant du train —

The issue at the origin of this work is the nature underlying the considerable gap (4.3 eV) of nickel oxide. The work presented in the thesis is divided in two main parts. The first part concerns the paramagnetic phase of NiO. In this phase, the Kohn-Sham LDA bands are metallic, however, LDA is not reliable for the calculation of excited-state properties. The main question about this phase was if exchange is able to open an insulating gap in NiO band structure. To answer this question I have carried out a Hartree-Fock (H-F) calculation. The paramagnetic phase turns out to be metallic also in the H-F approximation. At this point one should think for a moment at what is what we call "paramagnetic phase" and how it is modeled. To calculate a paramagnetic material means normally to consider a non-magnetic electronic structure. This means that the spin variable is not considered in the calculations. As a consequence, each band carries two spin-degenerate electrons. In other words, the spin-up and spin-down electronic densities are constrained to be exactly the same in every point of the system. This could be seen as an arbitray constraint, but it reflects the actual behaviour of several compounds, like e.g. silicon and other semiconductors, and in general of any non-magnetic material. I should add that all the method I used and presented here, simulate systems at 0 K. The temperature is not included as a part of the problem. The direct consequence is that what is normally called a paramagnetic, or a paramagnetic phase, should be called *zero-temperature* paramagnetic or better, diamagnetic. Actually, my calculations model the equivalent of a high-pressure NiO at 0 K, where the spin degeneracy is recovered by high value of pressure. Hence, the main conclusion to this first issue is that we are not capable to properly model the paramagnetic phase of nickel oxide and that we need to find an alternative approach.

We should think at the most general paramagnetic configuration, i.e. a *random* spin configuration, where the magnetic ordering has disappeared, but the spin has not. A possible way would be a supercell approach, where the spins could be able to put themselves in different configurations. This kind of system should definitely be closer to a high-temperature paramagnetic material. The H-F approximation was applied also to the anti-ferromagnetic phase of nickel oxide and gave a huge insulating gap (14 eV). This is not surprising, since HF is known to give highly overestimated gaps for bulk insulators and the anti-ferromagnetic phase of NiO is already slightly insulating (0.7 eV) in Kohn-Sham LDA. The overestimated band-gap is mainly due to the fact that in the Hartree-Fock approximation the screening of the system is neglected. An interesting fact concerning the magnetic ordering in NiO is that some people [18, 47] tried to calculate a ferromagnetic NiO in HF and other approximations. It turns out it is an insulator with gap values close to its anti-ferromagnetic counterpart. These studies suggest that the anti-ferromagnetic ordering is not the direct cause of the insulating band-gap, as one could conclude after having read Chapter 3. Apparently, it is necessary to have just *some* magnetic ordering, i.e. to treat the spin explicitly. It has been also suggested that in nickel oxide there could be some short-range magnetic ordering even above Néel's temperature. These arguments also encourage us to find a proper description of the high-temperature paramagnetic phase.

The second part of my work focused on the anti-ferromagnetic phase of nickel oxide. The attention is drawn particularly on the photoemission spectrum and on the energy-gap. In this part I made use of *ab-initio* theoretical methods derived from Many-Body Perturbation Theory (MBPT), such as the *GW* method. This method is normally used to calculate photoemission energy-gaps as first-order corrections to the Kohn-Sham LDA eigenvalues. The COHSEX approximation, a simplified version of *GW*, was used to achieve self-consistency in energies and wavefunctions. This approach was necessary since the Kohn-Sham LDA band structure was too poor to be used as a starting point for *GW* calculations, as also reported in literature. The main drawback of this step was computational, since the calculation time has increased by one order of magnitude with respect to *GW*. I believe this was particularly awkward because the whole of the valence bands was badly described in LDA. In fact, while in other materials like VO_2 [35] the problem turned out to concern mainly mixing between top-valence and bottom-conduction bands, the COHSEX valence wavefunctions are very different from their LDA counterparts. They are much more hybridized, not distinguishable between p and d types anymore. On the contrary, the bottom-conduction band appears to have even more d character. The high level of hybridization of the valence bands points out an issue concerning the description of NiO by means of the Hubbard model, that treats only the d bands, keeping the O p bands in a band picture. This e.g. the case of DMFT [48] and of LDA+DMFT [23, 24] approaches. In this sense, the Kohn-Sham

structure (within LDA or other approximations) favours too much this kind of approach. Although computationally heavier than standard *GW*, this self-consistent approach is much lighter than other self-consistent versions of *GW* like the so-called *QuasiParticle self-consistent GW* (QPscGW) [20]. At the same time, it remains reliable to describe properly the *GW* wavefunctions [34, 36]. In fact, my results for the photoemission spectrum are comparable with QPscGW results in literature [20]. The *GW*+COHSEX photoemission spectrum gives an energy-gap of about 5 eV.

I also applied vertex corrections to the self-energy in the $GW\Gamma$ approximation [37] and calculated the corrections for the COHSEX band-structure. The calculations showed that there is no marked difference in the photoemission spectrum with respect to the *GW*+COHSEX approach. Thus the RPA screening appears a reliable approximation, unlike what suggested by Faleev *et al.* [20], who ascribe the overestimation of the photoemission gap to a poor (i.e. RPA) approximation for the screening. It is also true that the $GW\Gamma$ approximation may not be accurate enough to improve sufficiently the screening.

This second part of my thesis will be a starting point for the analysis of neutral excitations with finite transferred momentum $\mathbf{q}$, namely the calculation of Inelastic X-ray Scattering (IXS) and Electron Energy-Loss Spectra (EELS). This kind of analysis could shed more light on the physics of NiO. In fact, the finite momentum transfer unveils the *d*-*d* excitations, which are forbidden for $\mathbf{q} = 0$. Lately, both theoretical and experimental communities are getting more and more interested in this kind of excitations in NiO and in other transition metal oxides. In fact, they exibit great excitonic effects for this kind of transition [25] that lie in the middle of the gap. Since the *d* states form the energy-gap, a proper description of the band-structure is mandatory to calculate energy-loss spectra. For the calculation of the spectra I will make use of Time-Dependent Density Functional Theory (TDDFT), that is a time-dependent extention of DFT, and of the Bethe-Salpeter Equation (BSE), that is a MBPT-derived method to calculate the polarizability of an electronic system.

To conclude, I studied nickel oxide by means of the "old-fashioned" Hartree-Fock method and of the advanced COHSEX+GW method, being able to get a lot of physical insight in both cases. The COHSEX+GW approach, applied for the first time on NiO, has given satisfactory results in good agreement with experimental data and coherent with other self-consistent many-body approaches. Moreover, the electronic structure will be a good starting point for an accurate analysis of the *d*-*d* excitations.

Appendix A

Special planes and points in the reciprocal space of the trigonal lattice

It's a tough job – but someone's got to do it.

When dealing with Brillouin zones, the task of finding high symmetry points can be non-trivial, especially if one is not dealing with simple and over-documented cubic lattices. This appendix is just a bit more than a *divertissement*, but the truth is that it is hard to find a concise and fully explanatory book or article that covers this particular subject for a rhombohedral lattice in a satisfactory manner.

With relatively simple notions of geometry and linear algebra it is possible to retrieve all planes and points of a Brillouin zone in the reciprocal space, following the definitions given in [41].

Planes embedded in $\mathbb{R}^3$

Properties

In three-dimensional Euclidean space, we may exploit the following facts that do not hold in higher dimensions:

- Two planes are either parallel or they intersect in a line.
- A line is either parallel to a plane or intersects it at a single point or is contained in the plane.
- Two lines perpendicular to the same plane must be parallel to each other.
- Two planes perpendicular to the same line must be parallel to each other.

Define a plane with a point and a normal vector

In a three-dimensional space, another important way of defining a plane is by specifying a point and a normal vector to the plane.

Let **p** be any known point in the plane, and let $\vec{n}$ be a nonzero normal vector to the plane. The desired plane is the set of all points **r** such that

$$\vec{n} \cdot (\mathbf{r} - \mathbf{p}) = 0. \tag{A.1}$$

If we write

$$\vec{n} = a\hat{\mathbf{x}} + b\hat{\mathbf{y}} + c\hat{\mathbf{z}} \qquad\qquad \mathbf{r} = x\hat{\mathbf{x}} + y\hat{\mathbf{y}} + z\hat{\mathbf{z}}, \tag{A.2}$$

where $\hat{\mathbf{x}}$, $\hat{\mathbf{y}}$, $\hat{\mathbf{z}}$ are the cartesian unit vectors (or direction vectors), and d as the dot product $d = -\vec{n} \cdot \mathbf{p}$, then the plane Π is determined by the condition

$$ax + by + cz + d = 0, \tag{A.3}$$

where a, b, c and d are real numbers and a, b, and c are not all zero.

Alternatively, a plane may be described parametrically as the set of all points of the form $\mathbf{r} = \mathbf{p} + s\vec{v} + t\vec{w}$, where s and t range over all real numbers, and **p** , $\vec{v}$ and $\vec{w}$ are given vectors defining the plane. **p** is the position vector from the origin to an arbitrary (but fixed) point on the plane, and $\vec{v}$ and $\vec{w}$ can be visualized as starting at **p** and pointing in different directions along the plane. $\vec{v}$ and $\vec{w}$ can, but do not have to be perpendicular (but they cannot be collinear).

Drawing planes in the Brillouin zone

The reciprocal space vectors are:

$$\begin{aligned}
\mathbf{G}_1 &= a_1\hat{\mathbf{x}} + b_1\hat{\mathbf{y}} + c_1\hat{\mathbf{z}} = (0.2069308, 0.0000000, 0.0366528) \\
\mathbf{G}_2 &= a_2\hat{\mathbf{x}} + b_2\hat{\mathbf{y}} + c_2\hat{\mathbf{z}} = (-0.1034654, 0.1792073, 0.0366528) \\
\mathbf{G}_3 &= a_3\hat{\mathbf{x}} + b_3\hat{\mathbf{y}} + c_3\hat{\mathbf{z}} = (-0.1034654, -0.1792073, 0.0366528)
\end{aligned} \tag{A.4}$$

Some special points are already known. They are:

- $\mathbf{L}_i^{\pm} = \pm\mathbf{G}_i/2$,
- $\mathbf{F}_i^{\pm} = \pm(\mathbf{G}_j + \mathbf{G}_k)/2$ with $i \neq j \neq k$.
- $\mathbf{T}^{\pm} = \pm(\mathbf{G}_1 + \mathbf{G}_2 + \mathbf{G}_3)/2$.

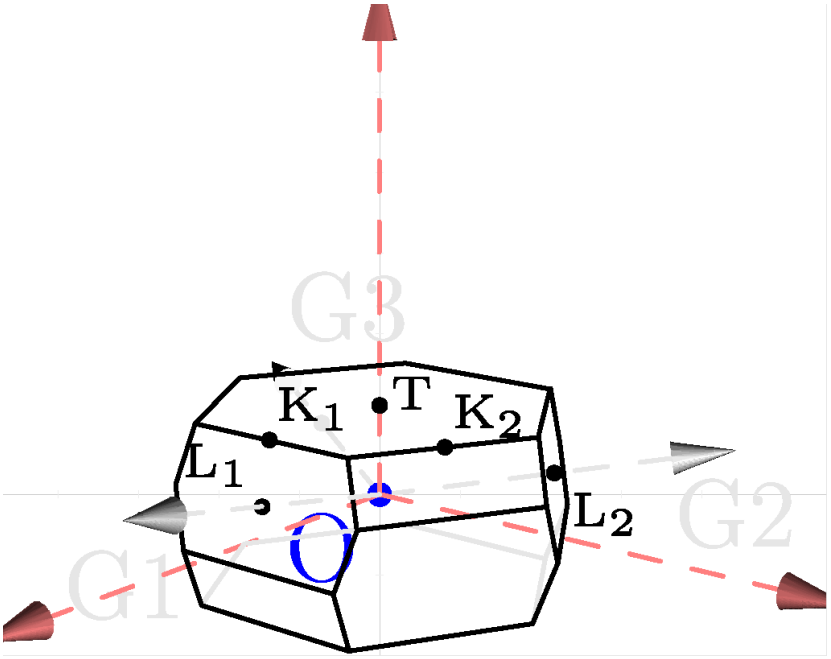

Figure A.1: Sketch of the first Brillouin's zone of a rhombohedral lattice. Some of the **L, K, T** special points are drawn.

Let's now consider the plane perpendicular to $\mathbf{G}_1$, that will be called $\Pi_{\mathbf{L}_1}$. In this case our normal vector $\vec{n}$ is $\mathbf{G}_1$ and the plane passes by $\mathbf{L}_1$. Thus, following the definitions given above, we get

$$\mathbf{p} = \frac{1}{2}\mathbf{G}_1 \qquad \mathbf{r} = x\hat{\mathbf{x}} + y\hat{\mathbf{y}} + z\hat{\mathbf{z}} \tag{A.5}$$

$$\vec{n} = \mathbf{G}_1 = a_1\hat{\mathbf{x}} + b_1\hat{\mathbf{y}} + c_1\hat{\mathbf{z}} \qquad d = -\vec{n}\cdot\mathbf{p} = -\frac{1}{2}\mathbf{G}_1\cdot\mathbf{G}_1 = -\frac{1}{2}|\mathbf{G}_1|^2. \tag{A.6}$$

The equation giving the plane is then

$$\Pi_{\mathbf{L}_1^+}: \quad a_1x + b_1y + c_1z - \frac{1}{2}|\mathbf{G}_1|^2 = 0. \tag{A.7}$$

Let's now take the plane normal to the direction $\mathbf{T}$ ($\hat{\mathbf{z}}$) passing by the point $\mathbf{T}^+$. We have

$$\vec{n} = \mathbf{G}_1 + \mathbf{G}_2 + \mathbf{G}_3, \qquad d = -\vec{n}\cdot\mathbf{p} = -\frac{1}{2}|\mathbf{G}_1 + \mathbf{G}_2 + \mathbf{G}_3|^2, \tag{A.8}$$

which yeld

$$\Pi_{\mathbf{T}^+}: \ (a_1 + a_2 + a_3)x + (b_1 + b_2 + b_3)y + (c_1 + c_2 + c_3)z - \frac{1}{2}|\mathbf{G}_1 + \mathbf{G}_2 + \mathbf{G}_3|^2 = 0. \tag{A.9}$$

Remarking that $(a_1 + a_2 + a_3) = (b_1 + b_2 + b_3) = 0$ the equation becomes

$$\Pi_{\mathbf{T}^+}: \quad (c_1 + c_2 + c_3)z - \frac{1}{2}|\mathbf{G}_1 + \mathbf{G}_2 + \mathbf{G}_3|^2 = 0. \tag{A.10}$$

Now is the turn of the plane perpendicular to $(\mathbf{G}_1 + \mathbf{G}_2)$ passing by the point $\mathbf{F}_3^+ = \frac{1}{2}(\mathbf{G}_1 + \mathbf{G}_2)$. With the same procedure as before we get

$$\vec{n} = \mathbf{G}_1 + \mathbf{G}_2, \qquad d = -\vec{n} \cdot \mathbf{p} = -\frac{1}{2}|\mathbf{G}_1 + \mathbf{G}_2|^2, \tag{A.11}$$

$$\Pi_{\mathbf{F}_3^+}: \quad (a_1 + a_2)x + (b_1 + b_2)y + (c_1 + c_2)z - \frac{1}{2}|\mathbf{G}_1 + \mathbf{G}_2|^2 = 0. \tag{A.12}$$

The last plane needed to have a decent set is a vertical plane passing by $\mathbf{G}_1$. It can be generated with the second method described before, as a plane generated by the $\hat{\mathbf{z}}$ vector and $\mathbf{G}_1$, i.e.

$$\Pi_{z_1} = t\hat{\mathbf{z}} + s\mathbf{G}_1 = t\begin{pmatrix}0\\0\\1\end{pmatrix} + s\begin{pmatrix}a_1\\b_1\\c_1\end{pmatrix} \tag{A.13}$$

which can be rewritten in canonical form as

$$\Pi_{z_1}: \quad b_1 x - a_1 y = 0, \tag{A.14}$$

that in this particular case, as $b_1 = 0$ simply becomes $y = 0$.

We may also need the vertical plane passing by $\mathbf{F}_3^+$, which has the following parametric form:

$$\Pi_{z_2} = t\hat{\mathbf{z}} + s(\mathbf{G}_1 + \mathbf{G}_2) = t\begin{pmatrix}0\\0\\1\end{pmatrix} + s\begin{pmatrix}a_1 + a_2\\b_1 + b_2\\c_1 + c_2\end{pmatrix} \tag{A.15}$$

which in the canonical form becomes

$$\Pi_{z_2}: \quad (b_1 + b_2)x - (a_1 + a_2)y = 0. \tag{A.16}$$

Changing the basis

In this section we define the basis changing matrix, which can transform a vector's coordinates from the cartesian base to our trigonal basis (A.4). Any vector $\vec{v}$ can

be represented in the cartesian reference ($\hat{\mathbf{x}}$, $\hat{\mathbf{y}}$, $\hat{\mathbf{z}}$) or in the trigonal reference ($\mathbf{G}_1$, $\mathbf{G}_2$, $\mathbf{G}_3$) as follows:

$$\vec{v} = a\hat{\mathbf{x}} + b\hat{\mathbf{y}} + c\hat{\mathbf{z}} = a^*\mathbf{G}_1 + b^*\mathbf{G}_2 + c^*\mathbf{G}_3. \tag{A.17}$$

The unit vectors can directly be used to build the basis change matrix which gives the cartesian coordinates given a point's trigonal coordinates. In a formula:

$$\mathbf{x}_{\text{cart}} = \mathbf{M} \cdot \mathbf{x}_{\text{tri}}. \tag{A.18}$$

The matrix is constructed, knowing the basis, as follows:

$$\mathbf{M} = (\mathbf{G}_1\mathbf{G}_2\mathbf{G}_3) = \begin{pmatrix} a_1 & a_2 & a_3 \\ b_1 & b_2 & b_3 \\ c_1 & c_2 & c_3 \end{pmatrix}. \tag{A.19}$$

The inverse matrix $\mathbf{M}^{-1}$ can be as well written, as it is the inverse of $\mathbf{M}$ and it obeys

$$\mathbf{x}_{\text{tri}} = \mathbf{M}^{-1} \cdot \mathbf{x}_{\text{cart}}, \tag{A.20}$$

which, expanded, is a little more complicated:

$$\begin{aligned} \mathbf{M}^{-1} = & \frac{1}{(a_1b_2c_3 - a_2b_1c_3 - a_1b_3c_2 + a_3b_1c_2 + a_2b_3c_1 - a_3b_2c_1)} \times \\ & \times \begin{pmatrix} b_2c_3 - b_3c_2 & a_3c_2 - a_2c_3 & a_2b_3 - a_3b_2 \\ b_3c_1 - b_1c_3 & a_1c_3 - a_3c_1 & a_3b_1 - a_1b_3 \\ b_1c_2 - b_2c_1 & a_2c_1 - a_1c_2 & a_1b_2 - a_2b_1 \end{pmatrix} \end{aligned}. \tag{A.21}$$

Putting the actual coefficients we can re-write the two matrices as:

$$\mathbf{M} = \begin{pmatrix} 0.2069308 & -0.1034654 & -0.1034654 \\ 0 & 0.1792073 & -0.1792073 \\ 0.0366528 & 0.0366528 & 0.0366528 \end{pmatrix}, \tag{A.22}$$

$$\mathbf{M}^{-1} = \begin{pmatrix} 3.221688925315451 & 0 & 9.094348408125255 \\ -1.610844462657726 & 2.79006491365028 & 9.094348408125255 \\ -1.610844462657726 & -2.79006491365028 & 9.094348408125255 \end{pmatrix}. \tag{A.23}$$

As we are forced to work in cartesian coordinates to operate with vectors, the basis change matrix is necessary to pass from the cartesian to the non-cartesian reference, and as we may have (and need) information in both references it becomes a precious tool to study the reciprocal space and in particular the Brillouin's zone.

Intersections of planes

Now we basically have all the planes that we need to find the special points that are missing. All we have to do is to intersect these planes and calculate the intersection points.

Point $\mathbf{K}_2$

Let us take first the planes Π_{z_2}, $\Pi_{\mathbf{F}_3^+}$ and $\Pi_{\mathbf{T}^+}$ and intersect them. This yelds the following system of equations:

$$\begin{cases} (b_1+b_2)x-(a_1+a_2)y=0 \\ (c_1+c_2+c_3)z-\dfrac{1}{2}|\mathbf{G}_1+\mathbf{G}_2+\mathbf{G}_3|^2=0 \\ (a_1+a_2)x+(b_1+b_2)y+(c_1+c_2)z-\dfrac{1}{2}|\mathbf{G}_1+\mathbf{G}_2|^2=0, \end{cases} \tag{A.24}$$

which becomes

$$\begin{cases} y=\dfrac{b_1+b_2}{a_1+a_2}x \\ z=\dfrac{|\mathbf{G}_1+\mathbf{G}_2+\mathbf{G}_3|^2}{2(c_1+c_2+c_3)} \\ x=\dfrac{(a_1+a_2)}{2}\dfrac{|\mathbf{G}_1+\mathbf{G}_2|^2-2(c_1+c_2)z}{(a_1+a_2)^2+(b_1+b_2)^2}. \end{cases} \tag{A.25}$$

Putting the numbers into this equations brings to the following result for the point we shall call $\mathbf{K}_2$:

$$\mathbf{K}_2^{(cart)}: \quad \begin{cases} x=0.048486619472184 \\ y=0.083981274529819 \\ z=0.0549792 \end{cases} \tag{A.26}$$

It can be interesting to know also the trigonal coordinates of $\mathbf{K}_2$ and, as we know that $\mathbf{K}_2^{(tri)}=\mathbf{M}^{-1}\cdot\mathbf{K}_2^{(cart)}$, applying $\mathbf{M}^{-1}$ we find

$$\mathbf{K}_2^{(tri)}: \quad \begin{cases} x=0.65620880497952 \\ y=0.65620880497952 \\ z=0.18758239004096 \end{cases} \tag{A.27}$$

Point $\mathbf{K}_1$

Let us now consider the point that we will call $\mathbf{K}_1$, which is at the intersection of planes Π_{z_1}, $\Pi_{\mathbf{L}_1^+}$ and $\Pi_{\mathbf{T}^+}$. The corresponding system of linear equations is

$$\begin{cases} y = 0 \\ (c_1 + c_2 + c_3)z - \dfrac{1}{2}|\mathbf{G}_1 + \mathbf{G}_2 + \mathbf{G}_3|^2 = 0 \\ a_1 x + b_1 y + c_1 z - \dfrac{1}{2}|\mathbf{G}_1|^2 = 0, \end{cases} , \tag{A.28}$$

$$\begin{cases} y = 0 \\ x = \dfrac{1}{a_1}\left(\dfrac{1}{2}|\mathbf{G}_1|^2 - c_1 z\right) \\ z = \dfrac{|\mathbf{G}_1 + \mathbf{G}_2 + \mathbf{G}_3|^2}{2(c_1 + c_2 + c_3)} \end{cases} . \tag{A.29}$$

Evaluating these expressions gives

$$\mathbf{K}_1^{(cart)} : \quad \begin{cases} x = 0.096973240554234 \\ y = 0 \\ z = 0.0549792 \end{cases} \tag{A.30}$$

and, as above,

$$\mathbf{K}_1^{(tri)} : \quad \begin{cases} x = 0.81241761514553 \\ y = 0.34379119242724 \\ z = 0.34379119242724 \end{cases} \tag{A.31}$$

Point $\mathbf{H}_1$

We now calculate the point $\mathbf{H}_1$, which is the intersection of planes $\Pi_{\mathbf{F}_3^+}$, $\Pi_{\mathbf{L}_1^+}$ and $\Pi_{\mathbf{T}^+}$. Here is the linear system:

$$\begin{cases} a_1 x + b_1 y + c_1 z - \dfrac{1}{2}|\mathbf{G}_1|^2 = 0 \\ (c_1 + c_2 + c_3)z - \dfrac{1}{2}|\mathbf{G}_1 + \mathbf{G}_2 + \mathbf{G}_3|^2 = 0 \\ (a_1 + a_2)x + (b_1 + b_2)y + (c_1 + c_2)z - \dfrac{1}{2}|\mathbf{G}_1 + \mathbf{G}_2|^2 = 0 \end{cases} . \tag{A.32}$$

Knowing that $b_1 = 0$ the system yelds

$$\begin{cases} z = \dfrac{|\mathbf{G}_1 + \mathbf{G}_2 + \mathbf{G}_3|^2}{2(c_1 + c_2 + c_3)} \\ x = \dfrac{1}{a_1}\left(\dfrac{1}{2}|\mathbf{G}_1|^2 - c_1 z\right) \\ y = \dfrac{1}{b_1 + b_2}\left[\dfrac{1}{2}|\mathbf{G}_1 + \mathbf{G}_2|^2 - (a_1 + a_2)x - (c_1 + c_2)z\right] \end{cases} . \tag{A.33}$$

Evaluating these expressions gives

$$\mathbf{K}_1^{(cart)} : \quad \begin{cases} x = 0.096973240554234 \\ y = 0.055987506168248 \\ z = 0.0549792 \end{cases} \tag{A.34}$$

and

$$\mathbf{K}_1^{(tri)} : \quad \begin{cases} x = 0.81241761514553 \\ y = 0.49999996899004 \\ z = 0.18758241586443 \end{cases} \tag{A.35}$$

Acknowledgements/Ringraziamenti

I would like to thank first of all my two "french" supervisors, Lucia and Matteo, who gave me the possibility to work with them and learn and have fun with physics in an always good, friendly, respectful and professional environment. I also would like to thank my "Italian" supervisor, Giorgio Benedek, who accepted to be my supervisor in Bicocca and left me free to do what I preferred, being always interested and available for help and discussion. I want to thank him also because it was also because of his course of structure of matter that I decided to direct my studies to solid-state physics a couple of years ago.

I must thank all the people at LSI-ETSF, who were always very friendly (sometimes too much! n'est-ce pas Julien?) and always ready to help me in and out the lab (merci Gaëlle!). You made me feel like I was in a new (though, truth told, a bit weird) family. :-)
Bon bah, écoutez, les remerciements en français peut-être dans la prochaine thèse, d'accord? En tout cas, un gran merci au LSI quoi! :-)

Grazie davvero a Lucia e Matteo, che mi hanno insegnato ad avere più fiducia e me ne hanno costantemente data, nonostante i miei ripetuti errori. Grazie per avermi contagiato con il vostro entusiasmo. Per la mia tesi di laurea non avrei potuto chiedere di meglio. Grazie al Prof. Benedek che è sempre stato per me un esempio di passione e divertimento nella e con la fisica. È doveroso un ringraziamento ulteriore a Matteo, che si è maggiormente speso per aiutarmi ed insegnarmi con una pazienza ed un rispetto veramente ammirevoli. Per non parlare della "assistenza" anche al di fuori del lab, e per via telematica, in Francia, Spagna ed Italia, che più volte è andata ben oltre il dovuto!

Ci sarebbero moltissime persone, incontrate nel corso degli anni universitari, da ringraziare a questo punto. Ne nominerò qui alcune. Ne dimenticherò sicuramente altre, ma questo non vuol dire che non abbiano dato un contributo seppur piccolo — ma non per questo meno importante — alla mia vita, che mi verrà alla mente in qualche momento inaspettato. Mi sento però di dire che è stato in questi anni che sono diventato "grande" e questo solo grazie alle persone che ho incontrato e che mi hanno dato un universo di idee, emozioni ed esperienze che poi fanno parte del bello della vita.

Grazie a tutti quei miei compagni di corso con cui ho condiviso le gioie dei cazzeggi e delle uscite universitarie e i dolori (e, non troppo spesso, le soddisfazioni) degli esami.

Grazie alla Cami, senza la quale ora potrei non essere laureando, che è sempre stata pronta a darmi un aiuto disinteressato. Grazie a Fra per avermi accolto per primo. Grazie a Rici, per le tante idee condivise, i tanti ottimi suggerimenti musicali e per una sintonia che ho trovato raramente con altri. Grazie alle persone che mi sono state vicine e che mi hanno arricchito e sostenuto in un anno difficile come il 2006/2007, tra gli altri, Alessandra, Dario, Fabri, Rici, la Cle, Teo, Jenny, la Fra, Claudia e Alice. Grazie a Eri per una amicizia che dura ancora nonostante tutto. Grazie a tutti gli astrofisicandi, per l'ospitalità nel periodo di tesi. Grazie a Nico (Il Biondo) per le dritte musicali e montanare. Grazie ai miei "compagni di erasmus", Giovanni, Francesca, Beppe (*io m'iscrivo ai terroristi!*), Erica e Elisa, con me in Francia o partiti come me da Milano per altri lidi, perché sia da vicino che da lontano sono riusciti a sostenermi e spero che alla fine ci siamo tutti sostenuti un po' a vicenda. Grazie alla Ire e a Giulia (plus Ire-colloc) per l'ospitalità e l'amicizia parigino-meratese. Grazie ai "vecchi" fisici che ci hanno accolto quando ancora c'era un'auletta al piano seminterrato, all'insegna di ciò che i francesi definirebbero *n'importe quoi*, ma aumentando in definitiva la nostra passione per la fisica (scusate, Fisica). Tra gli altri, il Barba, lo Ste Ravani, lo Ste Marelli, il Leo e Giordano. Grazie a Luigi per i Corti e per la sua campagna (meglio conosciuta come *La favola del treno*). Grazie a Bruce, Eli, Chiara, Gippo, Marchino, Carmen, Ema, Stefanino, Ste Kevin, Lore, Darione e tutti gli altri, che ora non ricordo (e siete tanti, ne sono certo!), ma con cui ho condiviso bei momenti ed emozioni. Anche grazie a voi sono riuscito ad arrivare fino a qui. Un ringraziamento particolare alle ragazze, perché da loro ho imparato che a volte è meglio rinunciare a capire. :-)

Un grazie infinito alla mia famiglia, per tutto l'amore che mi dà da sempre e per il sostegno incondizionato che mi regala. Penso qui anche ai familiari lontani e agli amici di famiglia che sono sempre pronti a dare una mano, per quanto possibile, in caso di necessità. Grazie ai miei genitori per il loro esempio (nel bene e nel male), i loro consigli e la loro dedizione assoluta. Grazie a mio fratello e a mia sorella, per aver sopportato fino ad ora i miei commenti non sempre concilianti e per aggiungere al mio orizzonte limitato dimensioni per me sempre nuove.

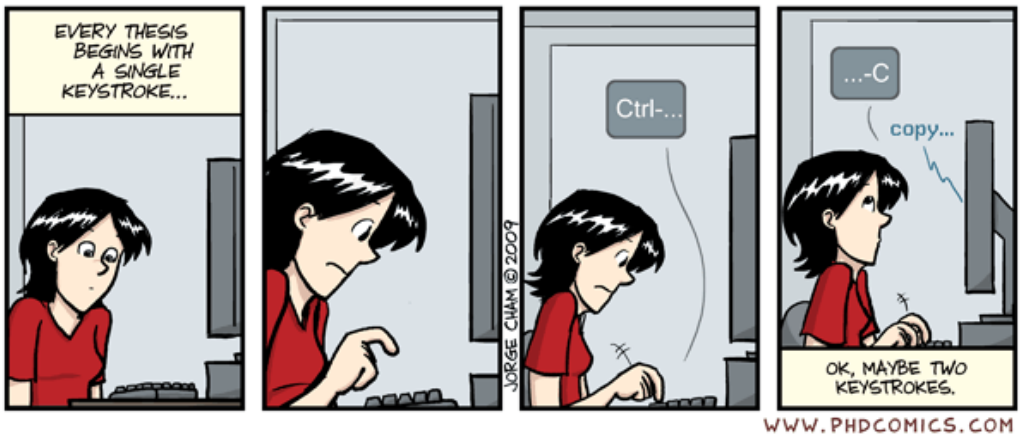
EVERY THESIS BEGINS WITH A SINGLE KEYSTROKE...
Ctrl-...
...-C
copy...
OK, MAYBE TWO KEYSTROKES.
JORGE CHAM © 2009
WWW.PHDCOMICS.COM

Bibliography

[1] Hohenberg, P. and Kohn, W., Phys. Rev. **136** (1964) B864 .

[2] Kohn, W. and Sham, L. J., Phys. Rev. **140** (1965) A1133.

[3] Fetter, A. L. and Walecka, J. D., *Quantum theory of Many-Particle Systems*, MacGraw-Hill, New York, 1971.

[4] Hedin, L., Phys. Rev. **139** (1965) A796.

[5] Hedin, L. and Lundqvist, S., *Solid State Physics*, volume 23, Academic Press, New York, 1969.

[6] Koopmans, T., Physica **1** (1933) 104.

[7] Sawatzky, G. A. and Allen, J. W., Phys. Rev. Lett. **53** (1984) 2339.

[8] Tjernberg, O. et al., Phys. Rev. B **54** (1996) 10245.

[9] Jauch, W. and Reehuis, M., Phys. Rev. B **70** (2004) 195121.

[10] Mott, N. F., *Metal–Insulator transitions — 2nd ed*, Taylor & Francis, London, 1990.

[11] Terakura, K., Williams, A. R., Oguchi, T., and Kübler, J., Phys. Rev. Lett. **52** (1984) 1830.

[12] Terakura, K., Oguchi, T., Williams, A. R., and Kübler, J., Phys. Rev. B **30** (1984) 4734.

[13] Mattheiss, L. F., Phys. Rev. B **5** (1972) 290.

[14] Mattheiss, L. F., Phys. Rev. B **5** (1972) 306.

[15] Shen, Z.-X. et al., Phys. Rev. B **44** (1991) 3604.

[16] Manghi, F., Calandra, C., and Ossicini, S., Phys. Rev. Lett. **73** (1994) 3129.

[17] Aryasetiawan, F., Gunnarsson, O., Knupfer, M., and Fink, J., Phys. Rev. B **50** (1994) 7311.

[18] Aryasetiawan, F. and Gunnarsson, O., Phys. Rev. Lett. **74** (1995) 3221.

[19] Massidda, S., Continenza, A., Posternak, M., and Baldereschi, A., Phys. Rev. B **55** (1997) 13494.

[20] Faleev, S. V., van Schilfgaarde, M., and Kotani, T., Phys. Rev. Lett. **93** (2004) 126406.

[21] Li, J.-L., Rignanese, G.-M., and Louie, S. G., Phys. Rev. B **71** (2005) 193102.

[22] Eguiluz, A. G. et al., J. Phys Chem. Sol. **66** (2005) 2281.

[23] Ren, X. et al., Phys. Rev. B **74** (2006) 195114.

[24] Kuneš, J., Anisimov, V., Lukoyanov, A. V., and Vollhardt, D., Phys. Rev. B **75** (2007) 165115.

[25] Larson, B. C. et al., Phys. Rev. Lett. **99** (2007) 026401.

[26] Haverkort, M., Tanaka, A., Tjeng, L. H., and Sawatzky, G. A., Phys. Rev. Lett. **99** (2007) 257401.

[27] Taguchi, M. et al., Phys. Rev. Lett. **100** (2008) 206401.

[28] Müller, F. and Hüfner, S., Phys. Rev. B **78** (2008) 085438.

[29] Lehmann, H., Nuovo Cimento **11** (1954) 342.

[30] Schwinger, J., Proc. Nat. Accad. Sci. **37** (1951) 452.

[31] Godby, R. W. and Needs, R. J., Phys. Rev. Lett. **62** (1989) 1169.

[32] http://www.abinit.org.

[33] Gonze, X. et al., Zeit. Kristallogr. **220** (2005) 558.

[34] Bruneval, F., *Exchange and Correlation in the Electronic Structure of Solids, from Silicon to Couprous Oxide:* GW *Approximation and beyond*, PhD thesis, École Polytechnique, Palaiseau (France), 2005.

[35] Gatti, M., *Correlation effects in valence-electron spectroscopy of transition-metal oxides : many-body perturbation theory and alternative approaches*, PhD thesis, École Polytechnique, Palaiseau (France), 2007.

[36] Bruneval, F., Vast, N., and Reining, L., Phys. Rev. B **74** (2006) 045102.

[37] Del Sole, R., Reining, L., and Godby, R. W., Phys. Rev. B **49** (1994) 8024.

[38] Slater, J. C., Phys. Rev. **82** (1951) 538.

[39] Hubbard, J., Proc. Roy. Soc. A **276** (1963) 238.

[40] von Barth, U. and Hedin, L., J. Phys. C: Solid State Phys. **5** (1972) 1629.

[41] Ashcroft, N. W. and Mermin, N. D., *Solid state physics*, Holt, Rinehart and Winston, New York, 1976.

[42] Troullier, N. and Martins, J. L., Phys. Rev. B **43** (1991) 1993.

[43] Kleinman, L. and Bylander, D. M., Phys. Rev. Lett. **48** (1982) 1425.

[44] http://www.fhi-berlin.mpg.de/th/fhi98md/fhi98PP.

[45] Monkhorst, H. J. and Pack, J. D., Phys. Rev. B **13** (1976) 5188.

[46] Holm, B. and von Barth, U., Phys. Rev. B **57** (1998) 2108.

[47] Patterson, C. H., Int. J. of Quantum Chem. **106** (2006) 3383.

[48] Georges, A. and Kotliar, G., Phys. Rev. B **45** (1992) 6479.